



# Detection Systems





# Detection Systems

## Requirements:

- Good energy resolution for Compton scattering rejection
- High detection efficiency for radionuclides of interest
- Sufficient spatial resolution so that it does not limit overall system resolution
- Low dead-time at count rates of interest

# Conventional Anger Camera

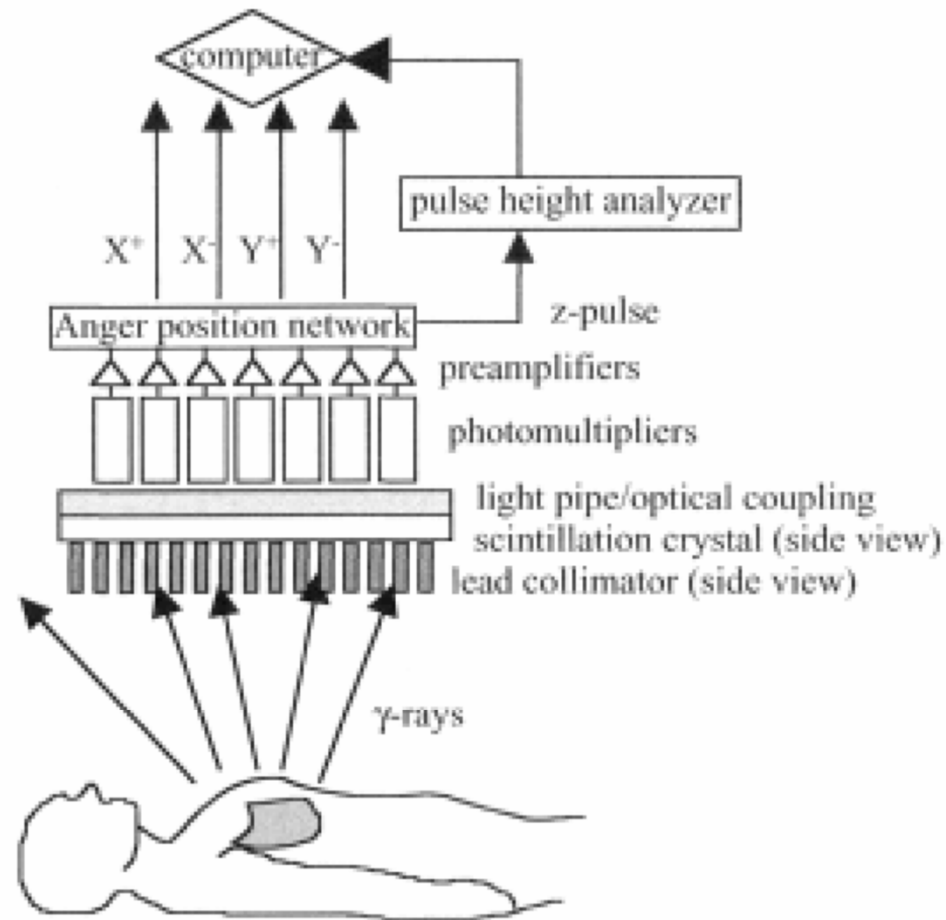
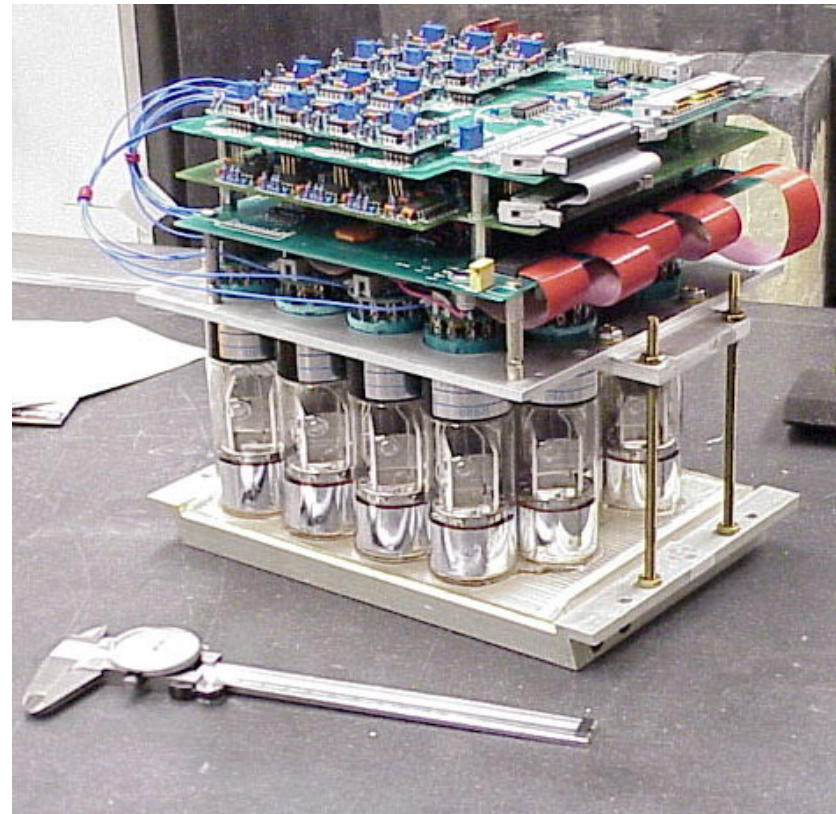


**FIGURE 2.4.** Schematic diagram of a gamma camera positioned above the patient. The distribution of the radiopharmaceutical is indicated by the shaded region within the body.

# Conventional Anger Camera

- PMTs coupled to large, continuous NaI(Tl) crystal
- Spatial resolution 3–4 mm FWHM
- Energy resolution 8–10% FWHM
- Mature technology (DoB ~1957)
- Large-area, >40cm x 40cm typical
- Simple and cost-effective



SPRINT II camera module



## Scintillation Crystal Used in Gamma Cameras

- Crystal (typically NaI) scintillates with blue light in a linear fashion related to gamma ray energy.
  - Grown crystal
  - Hydroscopic ( $H_2O$  sensitive)
- Thickness used depends upon energy measured. Thickness goes up as energy increases
- 13% of gamma energy  $\rightarrow$  light
- New detector technology uses solid state crystals – Cadmium Zinc Telluride (CZT)

# Scintillation Crystal Properties

TABLE 1 Properties of Common Scintillation Crystals Used in Small-FOV Imager Designs

Scintillator	Effective Z	Density (g/cc)	Radiation Length (mm) <sup>a</sup>	Relative Light Yield	Refractive Index	Decay Time (ns)	Peak Emission Wavelength (nm)	Hygroscopic?	Rugged?
NaI(Tl)	51	3.67	3.4	100	1.85	230	410	Yes	No
CsI(Tl)	54	4.51	2.2	135	1.79	1000	530	No	Yes
CsI(Na)	54	4.51	2.2	75	1.79	650	420	No	Yes
BGO	74.2	7.13	10.5	15	2.15	300	480	No	Yes
LSO(Ce)	65.5	7.4	11.6	75	1.82	40	420	No	Yes
CaF <sub>2</sub> (Eu) <sup>b</sup>	16.9	3.17	N/A	50	1.43	940	435	No	Yes

<sup>a</sup>Radiation lengths for NaI(Tl), CsI(Tl) and CsI(Na) are for 140-keV photons; Values for BGO and LSO are at 511 keV.

<sup>b</sup>CaF<sub>2</sub>(Eu) is used in beta imaging.

Detection efficiency

No. of visible photons per interaction

Efficiency for converting the light signal to electronic signal

# Scintillation Light

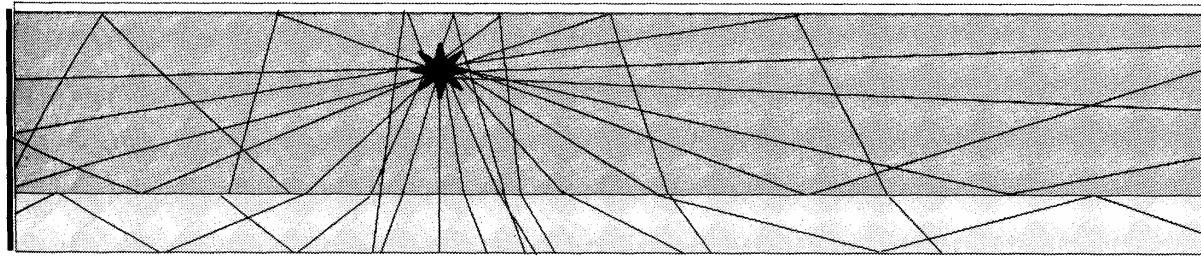


**FIGURE 4** Representation of light ray propagation from a point source of light within a scintillation crystal slab with a white diffuse Lambertian reflector on top, absorbing sides, and a light diffuser on the bottom leading into the photodetector.

- Scintillation light are generated isotropically.
- It is difficult to control light propagation inside a continuous bulk scintillator
- Light spreading leads to loss in both spatial resolution and energy resolution.
- Normally, the best we can do is to provide a better boundary condition for a better light collection efficiency.

# Scintillation Photons Emitting from the Crystal

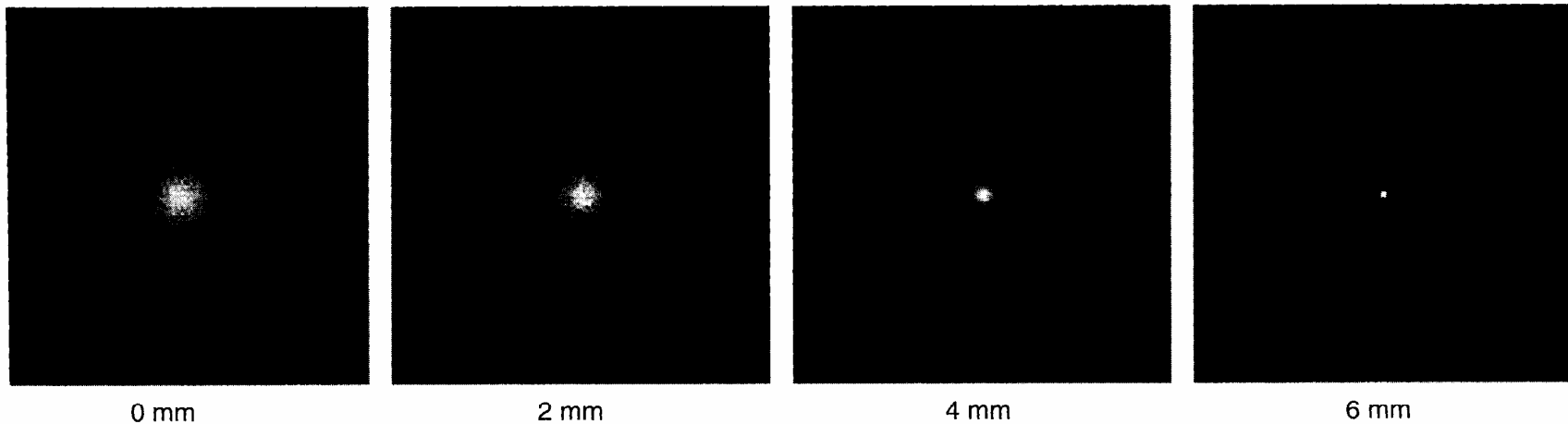


FIGURE 5 Light distribution seen at bottom of a  $6 \times 6 \times 0.6 \text{ cm}^3$  NaI(Tl) crystal for four depths from the top of the crystal of a point light source. The light spread widths are 9.2, 7.2, 3.5, and 0.7 mm FWHM, respectively.

light distribution shared over multiple photodetector elements with an Anger-type positioning scheme is governed by Poisson statistics (Tanaka *et al.*, 1970; Barrett and Swindell, 1981):

$$R_{\text{lim}} = 2.35 \left( \sum_i \frac{(dn_i / dx)^2}{n_i} \right)^{-1/2} \quad (4)$$

An optional observation:

$n_i$  is the number of photons at the  $i$ th spatial location. Suppose we know the distribution of the light pool, so we can derive how the no. of photons changing with spatial location  $x$ .

# Continuous and Discrete Crystals

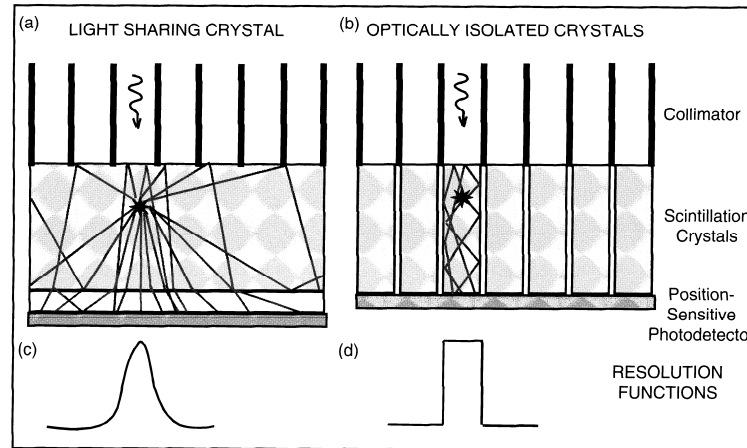


FIGURE 6 Schematic drawings of the light ray propagation for typical (a) single and (b) multiple scintillation crystal camera designs. For the pixellated design, scintillation light is confined to one crystal and focused on one spot of the photodetecting array. (c,d) Approximate shapes of the resulting theoretical intrinsic point spread functions for single-photon imaging.

## Continuous:

- Photons reaching detector surface after a few reflection or refraction – better light collection efficiency.
- Light spread is wide → (a) poor resolution (b) suffers from detector non-uniformity.

## Discrete:

- Multiple reflection before collection.
- Light collection is degraded → depending on interaction depth.
- Internal (total) reflection is the best way to key the photon inside.

# The Light Transport in Discrete Crystals

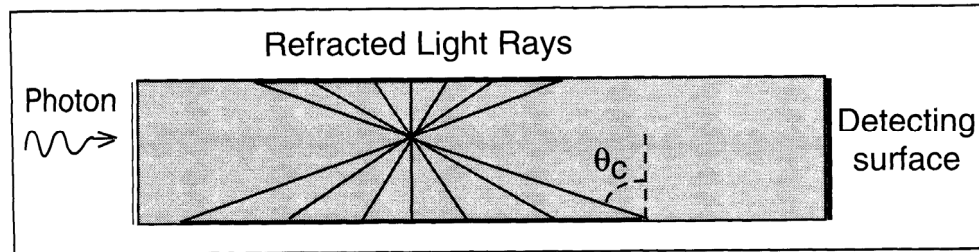
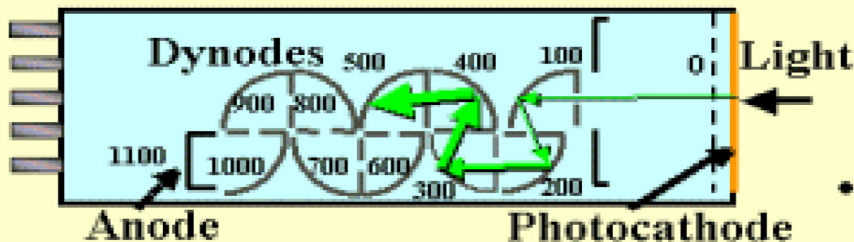


FIGURE 7 Depiction of the fraction of scintillation light lost from refraction through the sides of a long and narrow scintillation crystal for all incident angles less than the critical angle,  $\theta_c$ . High-energy photons enter the crystal from the left and only a fraction of the scintillation light created is piped down to the detecting surface at the right.

- Air gap is maintained around the side walls of each elements.
- Crystals with larger refraction index provide better light collection.

# The Photomultiplier Tube

## Photomultiplier Tube (PMT)



- Converts visible light (scintillation) into an electronic pulse
- Electron amplification through a series of dynodes
- Overall gain  $\sim 10^6$

Light hitting the photocathode liberates electrons which are accelerated through a series of dynodes. The electron gain at each dynode is  $\sim 4$ .

# The Photomultiplier Tube

## Other electron multiplication structures

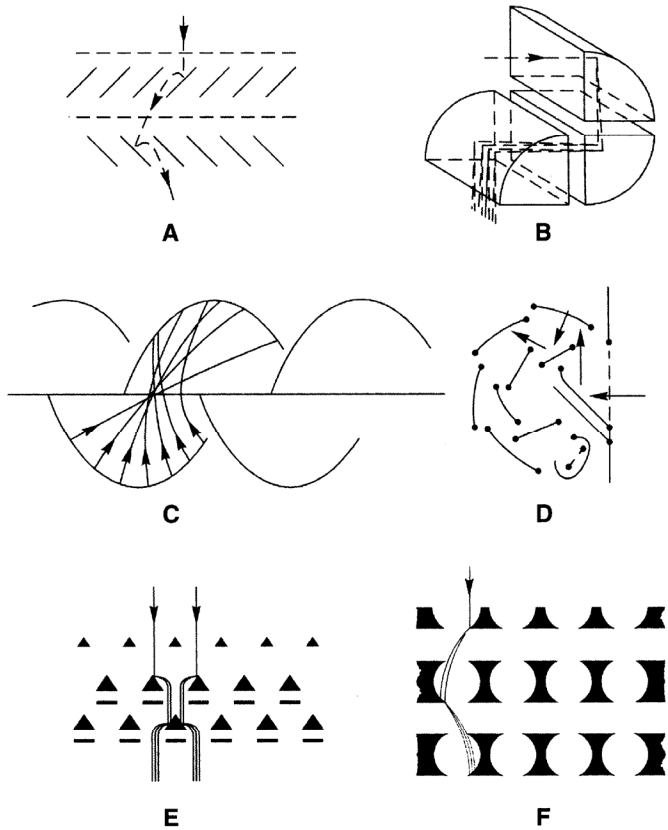


FIGURE 2 Scheme of dynode configurations: (a) venetian blind dynodes, (b) box dynode structure, (c) linear focusing dynodes, (d) circular cage dynodes, (e) mesh dynodes, and (f) foil dynodes. (From Photonis, 1994, *Photomultiplier Tubes: Principles and Applications*.)

## Typical power supply unit

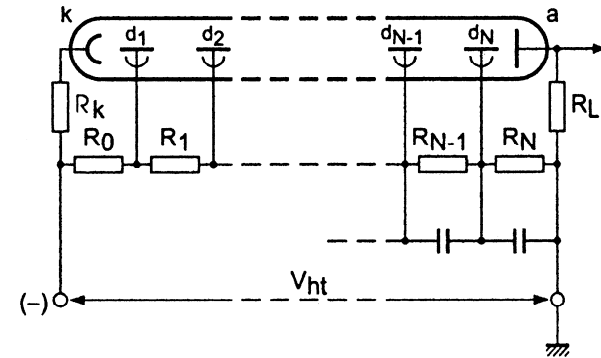


FIGURE 4 High-voltage PMT resistor network with the anode grounded and the cathode at negative high-voltage polarity. (From Photonis, 1994, *Photomultiplier Tubes: Principles and Applications*.)

- PMTs has gone through many generations.
- They are simple, robust and in many cases reasonably cost-effective.

The down side:

- Relatively low quantum efficiency → only 1 in 5 incident photons are converted to photonelectron.

# Position Sensitive Photomultiplier Tubes

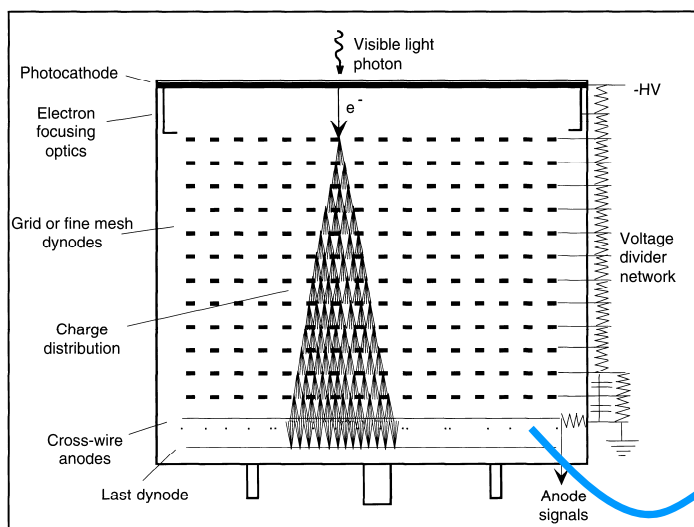


FIGURE 11 Depiction of the cross-wire anode PSPMT and its signal formation process. For simplicity, the charge avalanche created from only a single photoelectron is shown. A  $10^5$  photoelectron amplification factor is typical. Setting the cathode at ground and biasing the anode at +HV through a coupling capacitor is also possible.

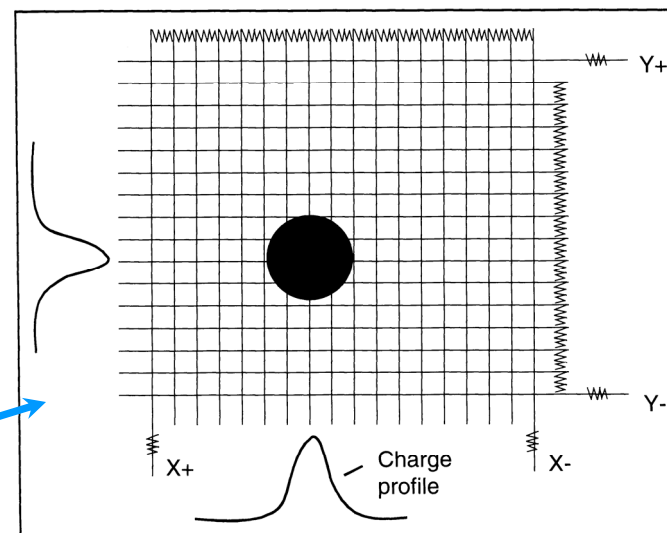


FIGURE 13 Example depiction of resistive charge division readout scheme for event positioning with a cross-wire anode PSPMT.

The cross-wire readout circuitry

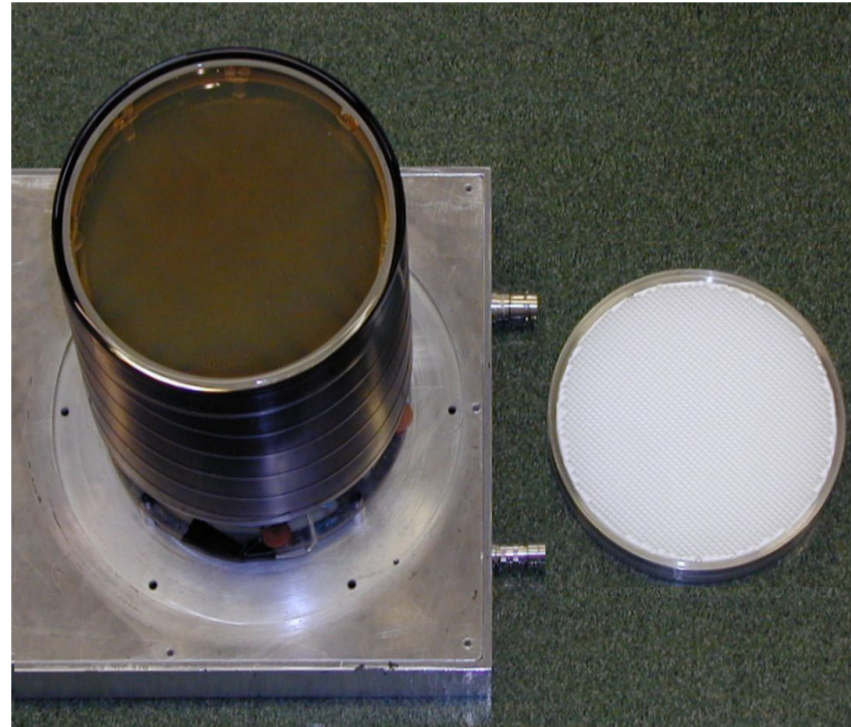
# PSPMT + Pixellated Scintillator

## Advantages

- Small size useful for niche applications
- Pixellated scintillator → high spatial resolution

## Disadvantages

- Quantum efficiency ( $\sim 25\%$ )
- Pixellated scintillator has poorer energy resolution ( $>10\%$ ) than continuous
- Small size is inadequate for many applications (human SPECT)
- Expensive!



# Modern Readout Electronics for Scintillation Cameras

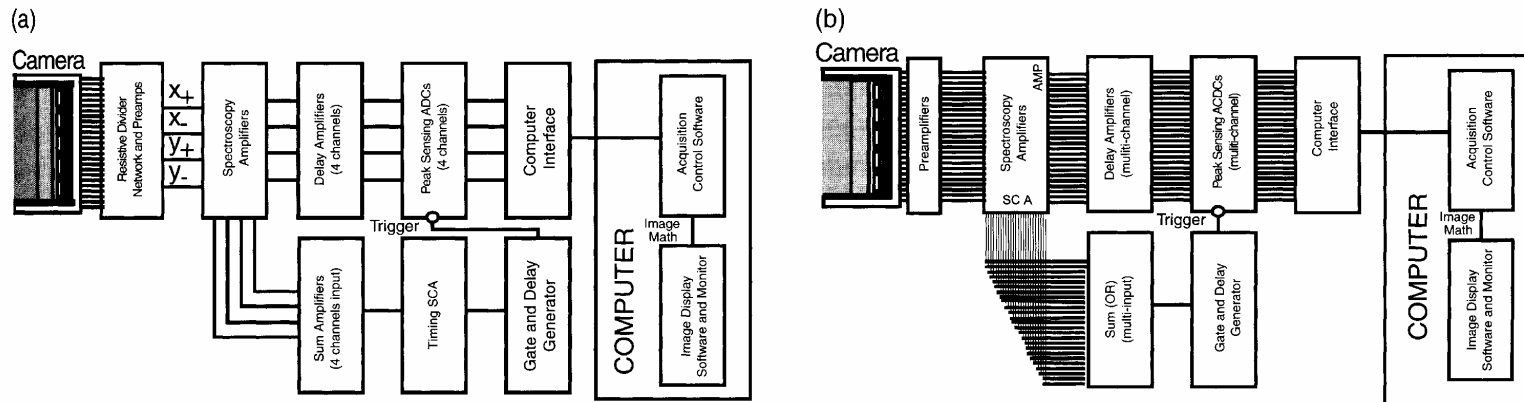


FIGURE 14 Basic examples of electronic processing topologies for image acquisition for the (a) resistive charge division readout and (b) parallel readout schemes.

Two flavors: charge sharing scheme and fully discrete readout methods

# The Readout Electronics for Photomultiplier Tube

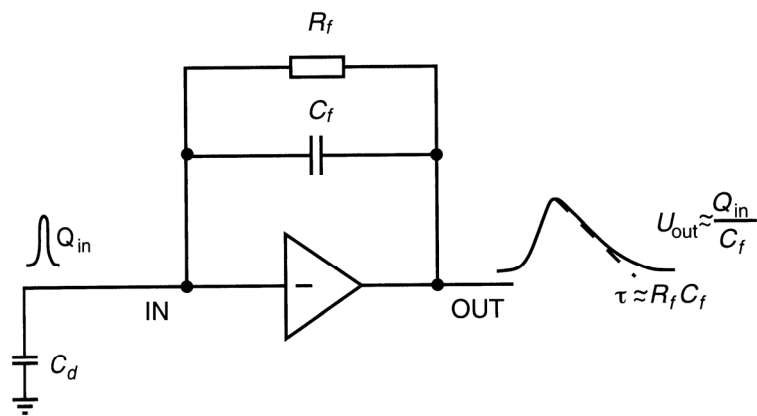


FIGURE 5 Basic circuit diagram of a charge-sensitive preamplifier. The charge of the detector capacitance  $C_d$  is converted into a voltage signal  $U_{out}$ .

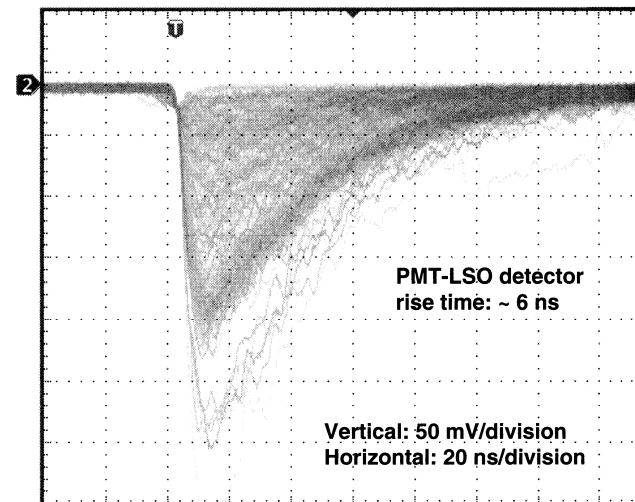


FIGURE 3 Output signal shape of a LSO-PMT detector.

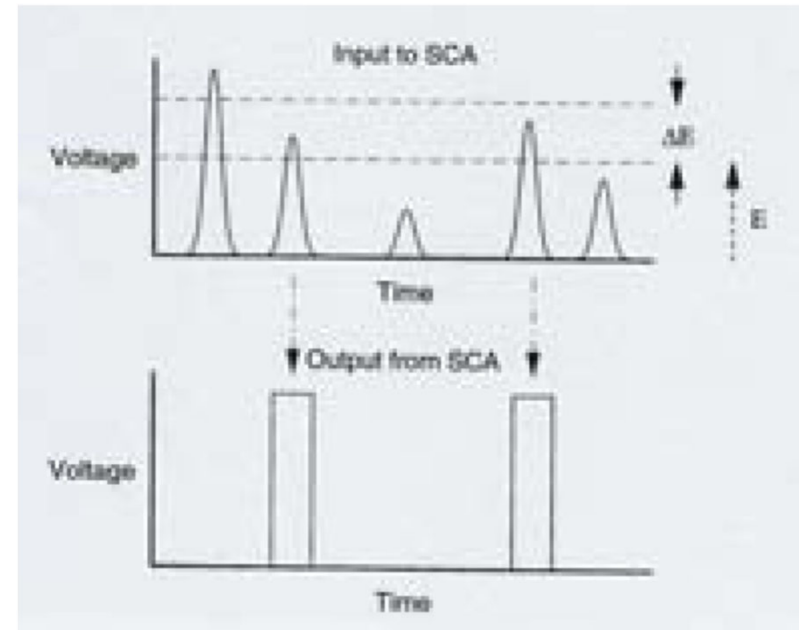
Charge amplifier circuitry for PMTs

Typical pulse waveform

# Extracting Energy Information from Scintillation Cameras

The simplest form of data acquisition: photon counting with single channel analyzers

- Pulse comes in sequence.
- A readout circuitry having 2 threshold.
- It pick up those events with signal amplitudes falling between the two threshold levels.
- The output of the SCA is the no. of events that have their signal amplitudes satisfy this condition.





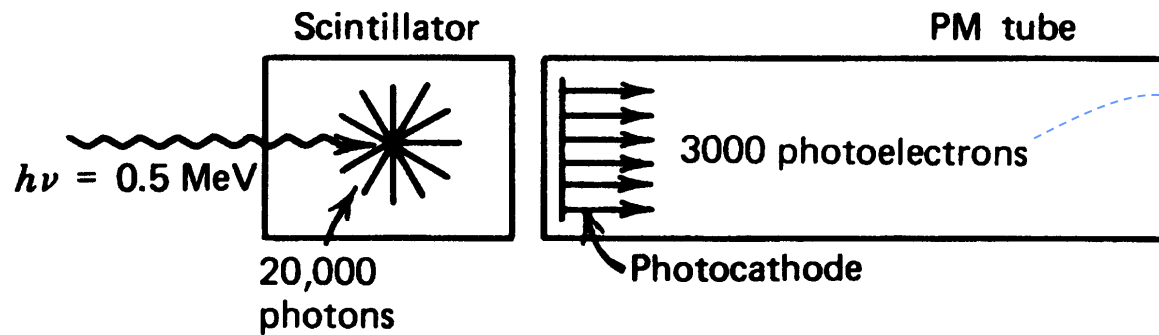
# Importance of Energy Information

- Now considering we have many single-channel analyzer (SCA) having their windows cover a wide energy ranges, what would we have?
- Converting the pulse amplitude into a digital value is called digitization. This is done using the Analogue-to-Digital Converter (ADC).

Just how well can we determine the energy of an incident gamma ray?

For details on energy information from scintillation detectors, please refer to Chapter 10, Page 307-334 in Radiation Detection and Measurements by G. F. Knoll.

# Further Broadening in Energy Spectrum



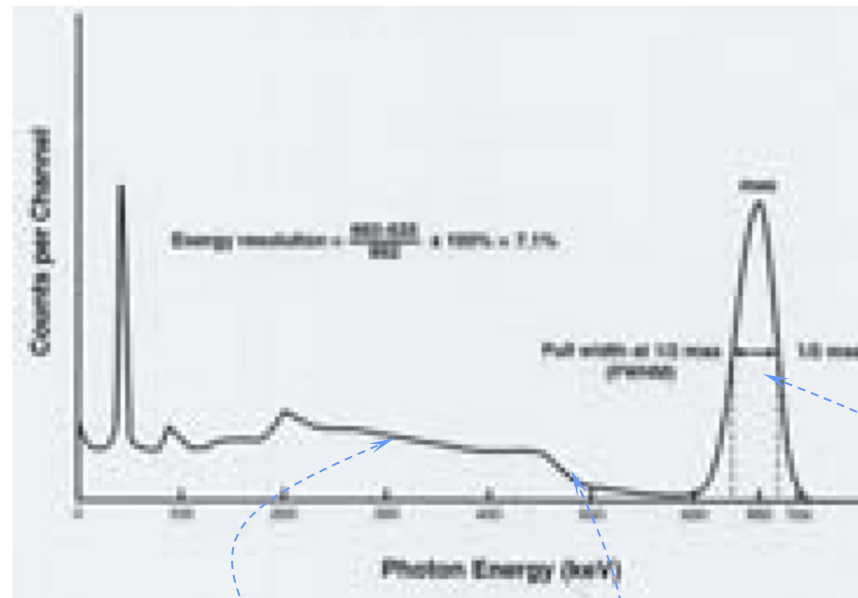
The number of photoelectrons  $\rightarrow$  a Poisson variable

Energy resolution due to Poisson fluctuation on the number of photoelectrons

$$R \equiv \frac{\text{FWHM}}{H_0} = K \frac{\sqrt{E}}{E} = \frac{K}{\sqrt{E}}$$

where  $K$  is a constant of proportionality. The energy resolution should thus be inversely proportional to the square root of the gamma-ray energy.

# Typical Energy Resolution at 662keV



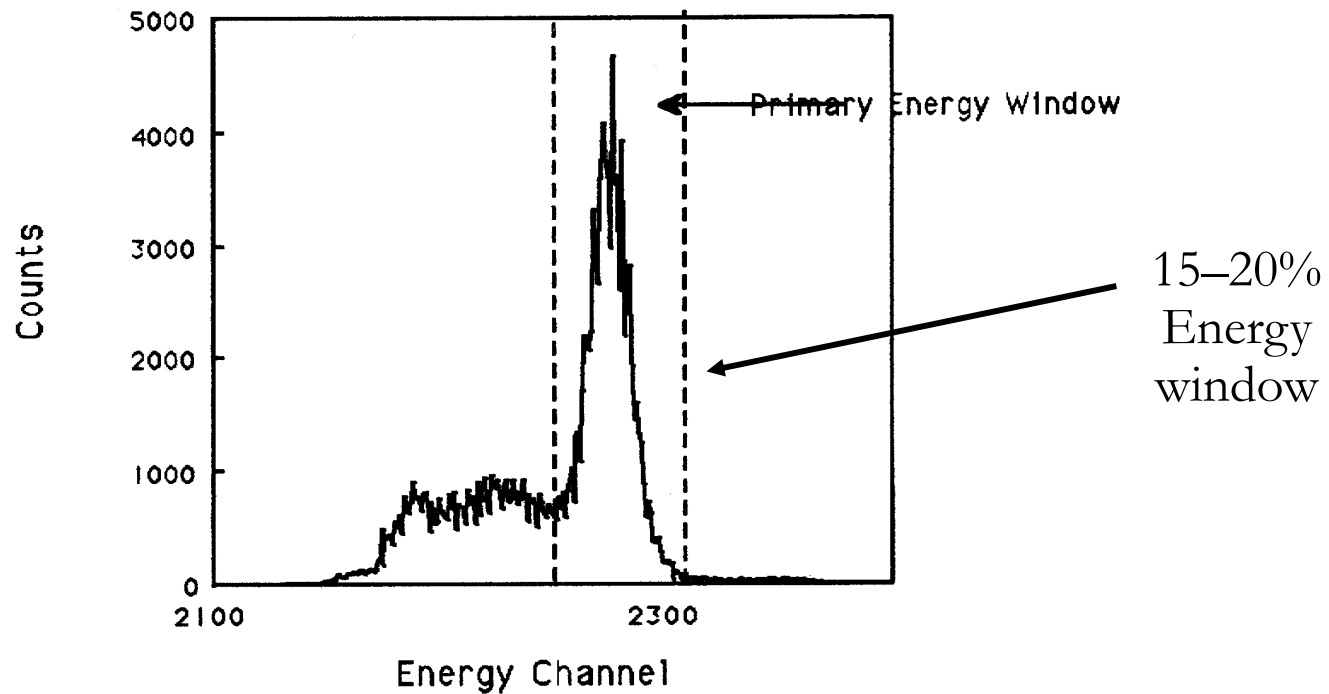
The Compton continuum → Events that interact in the detector but only deposited part of their energy.

The photopeak → normally contains a fraction of detected events

The Compton edge → Events that Compton scattered in the detector with a large scattering angle (say >120 degrees) and then the scattered photon escape from the detector.

Corresponding to the greatest energy loss by a photon through a single Compton scattering.

## Camera Energy Spectrum at 140 keV



Typical Anger camera has from 8–10% FWHM energy resolution at 140 keV

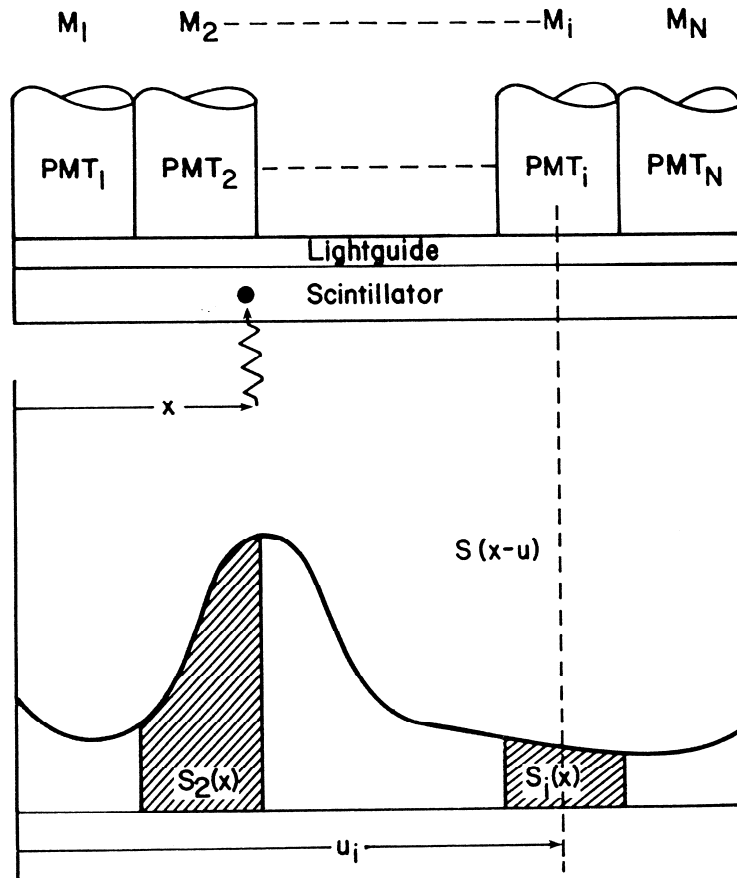


## Factors Affecting the Energy Resolution

- The crystal light-yield non-linearity → # of photons per unit energy deposition depends on photon energy.
- Light collection non-uniformity due to imperfections on the scintillation crystal.
- Photocathode non-uniformity of the PMT used.
- Statistical fluctuation on the # of photoelectrons generated.
- Readout electronic noise.

Better energy resolution is crucial for scattering rejection.

# Estimating Interaction Position



Energy:

$$\hat{E} = \sum_{i=1}^N M_i$$

Position:

$$\hat{x} = \frac{\sum_{i=1}^N c_i M_i}{\sum_{i=1}^N M_i}$$

$c_i$  –  $x$  coordinate of  $i$ -th phototube

We would need to know the signal amplitude from each PMT to estimate the energy and position ...

## The Charge Sharing Scheme

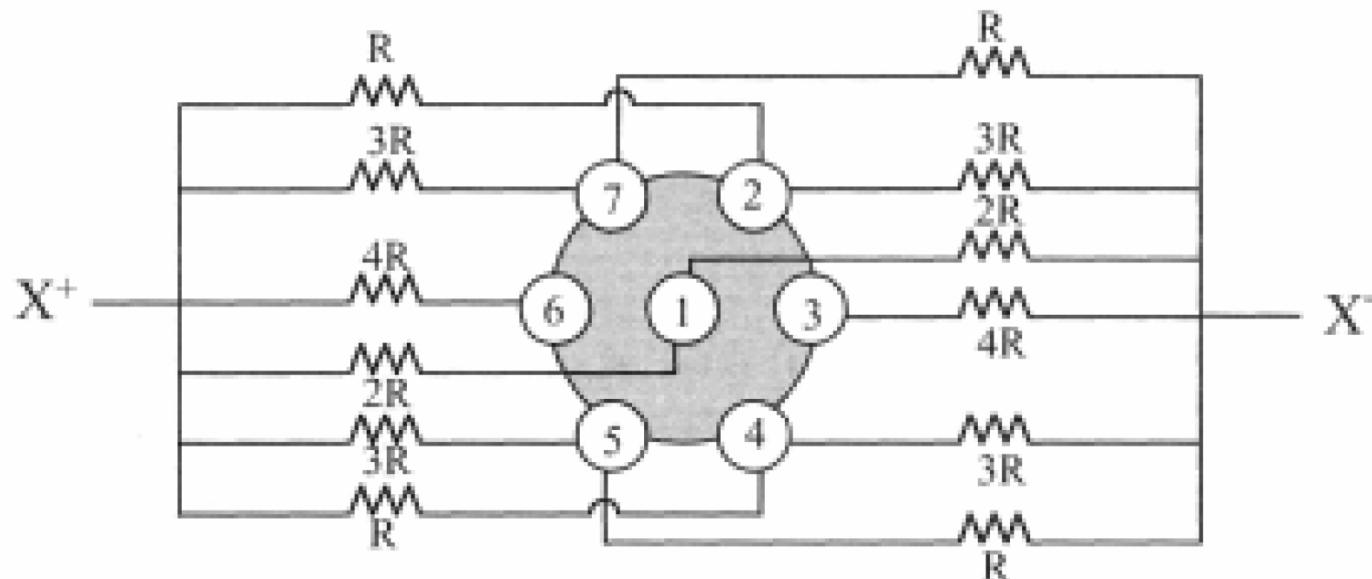
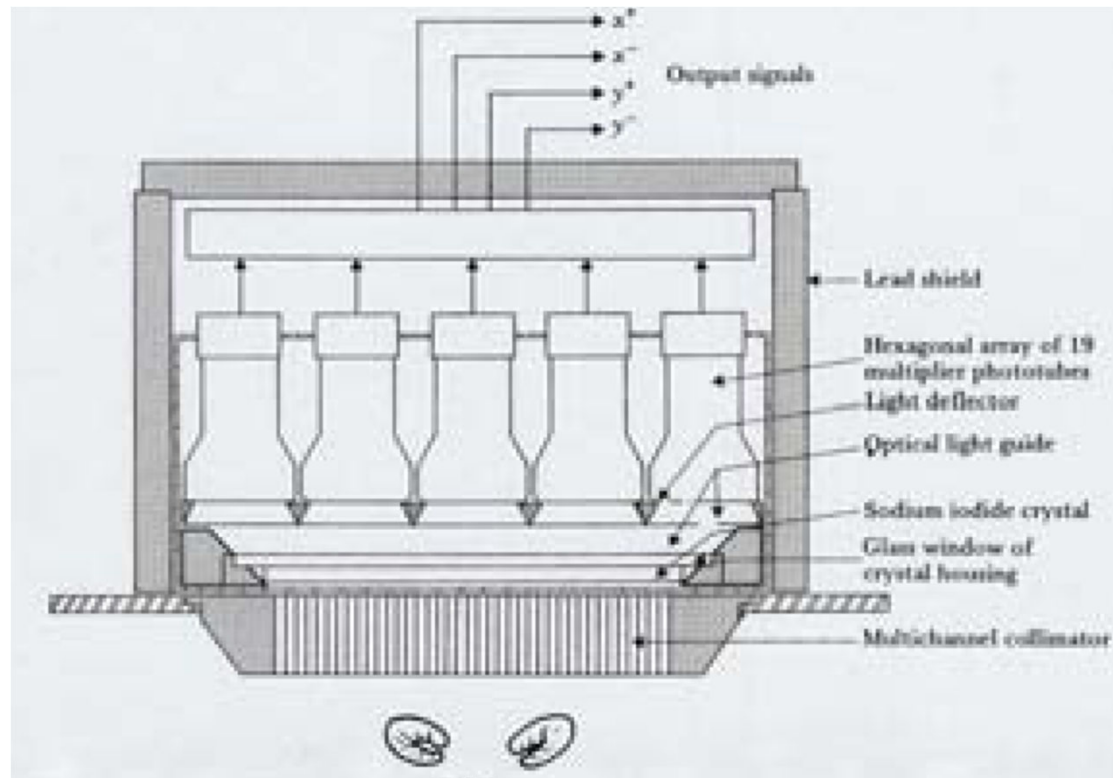


**FIGURE 2.8.** A version of an electronic network used for estimating the location at which a particular  $\gamma$ -ray strikes the scintillation crystal. For simplicity, only the  $X^+$  and  $X^-$  channels are shown in their entirety and only seven PMTs (1–7) are drawn. The magnitude and polarity of the outputs  $X^+$  and  $X^-$  determine the position estimate in the  $x$  direction.

# The Charge Sharing Scheme



$$x_c = \frac{x^- - x^+}{x^- + x^+}$$

$$y_c = \frac{y^- - y^+}{y^- + y^+}$$

# Scintillation Crystal Properties

TABLE 1 Properties of Common Scintillation Crystals Used in Small-FOV Imager Designs

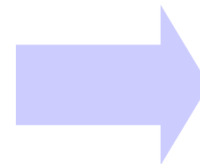
Scintillator	Effective Z	Density (g/cc)	Radiation Length (mm) <sup>a</sup>	Relative Light Yield	Refractive Index	Decay Time (ns)	Peak Emission Wavelength (nm)	Hygroscopic?	Rugged?
NaI(Tl)	51	3.67	3.4	35,000/MeV 100	1.85	230	410	Yes	No
CsI(Tl)	54	4.51	2.2	135	1.79	1000	530	No	Yes
CsI(Na)	54	4.51	2.2	75	1.79	650	420	No	Yes
BGO	74.2	7.13	10.5	15	2.15	300	480	No	Yes
LSO(Ce)	65.5	7.4	11.6	75	1.82	40	420	No	Yes
CaF <sub>2</sub> (Eu) <sup>b</sup>	16.9	3.17	N/A	50	1.43	940	435	No	Yes

<sup>a</sup>Radiation lengths for NaI(Tl), CsI(Tl) and CsI(Na) are for 140-keV photons; Values for BGO and LSO are at 511 keV.

<sup>b</sup>CaF<sub>2</sub>(Eu) is used in beta imaging.

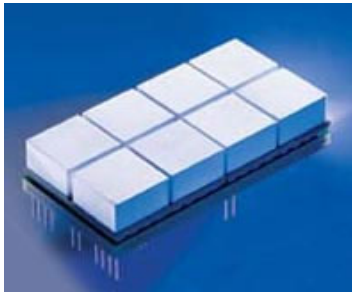
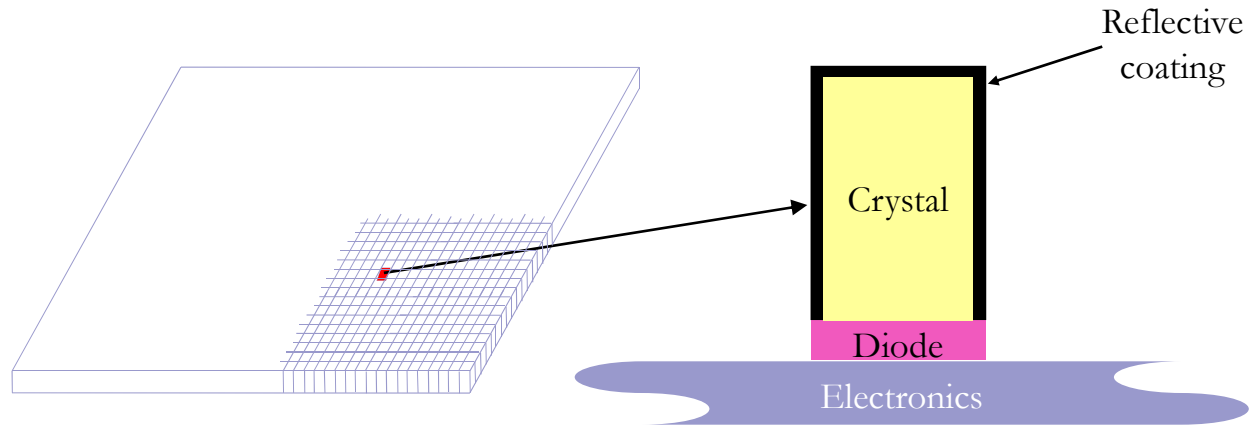
Consider

- 100keV produces 3500 photons
- 40% light collection
- 20% quantum efficiency (photoelectron/photon)



Total signal generated on the PMT:  
280 photoelectrons

# Detector Technology for Improving Spatial Resolution – Discrete Detector Elements



Eight modules in array

- Pixellated CsI(Tl) scintillator separated by reflector
- Arrays of PIN photodiodes and readout electronics

Drawing courtesy Jerome Gormley, Digirad, Inc

# Standard Photodiode Sensor

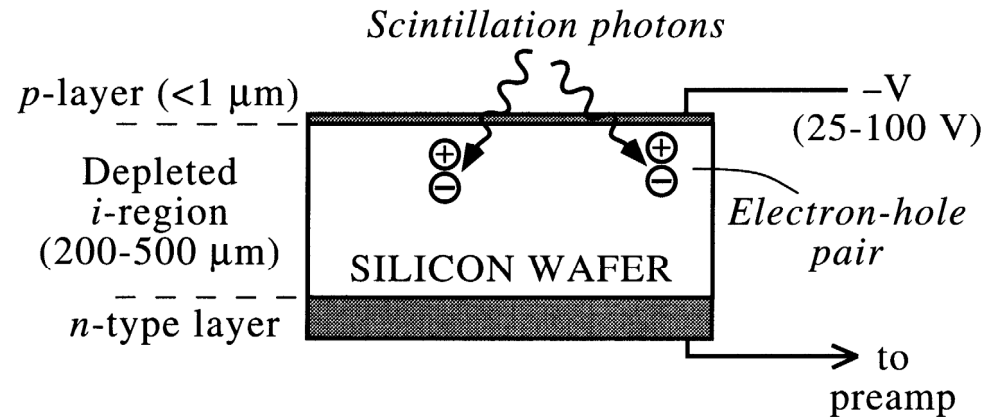
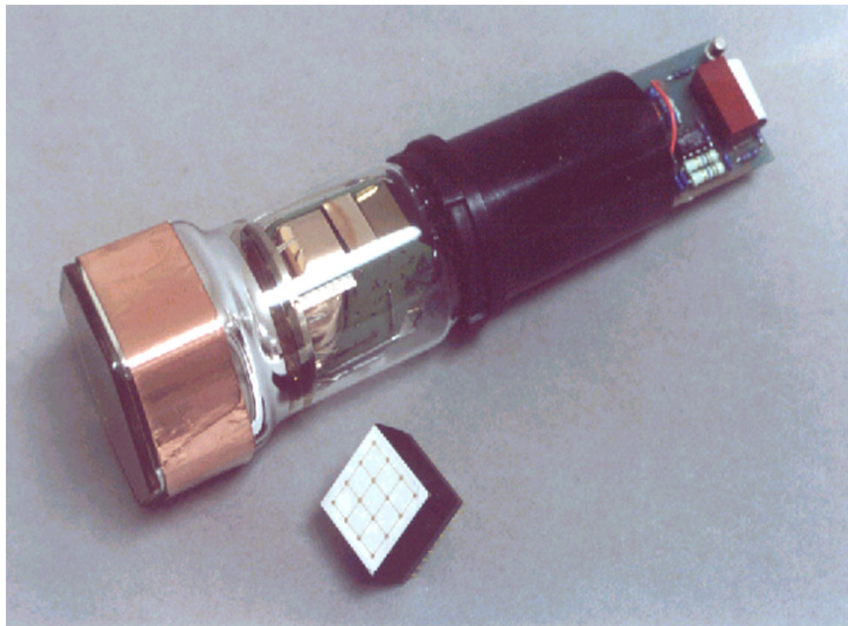


**Figure 9.14** Basic configuration of a conventional photodiode.

- Visible photon sensor
- Very good quantum efficiency  $\rightarrow$  90% of incident photons can be converted to photoelectron.
- PD: No internal gain  $\leftrightarrow$  PMT: gain  $\sim$  1 Million
- Page 287, G F Knoll, Radiation Detection and Measurements for details.

# PIN Photodiode + CsI(Tl) Scintillator



Comparison of Photodiode/CsI(Tl) module with PMT used in Anger camera

Photo courtesy Jerome Gormley, Digirad, Inc

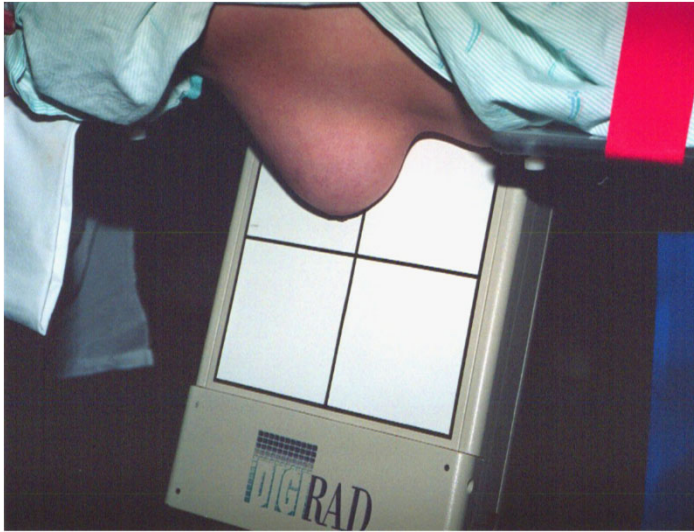
## Advantages

- Size
- High quantum efficiency—  $>80\%$  vs.  $25\%$  for PMT/NaI(Tl)
- Excellent spatial resolution

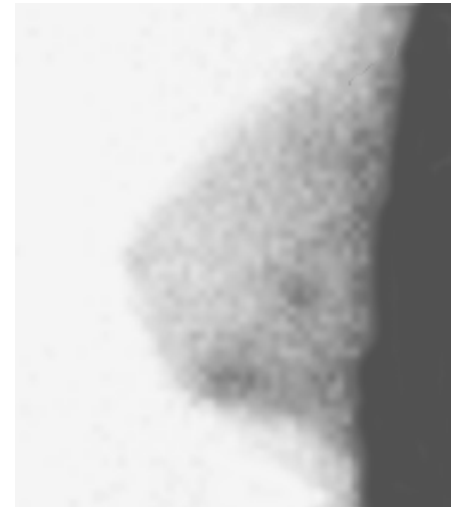
## Disadvantages

- No internal gain, therefore noisier compare with PMT.
- Modest energy resolution
- Not cheap!

# Solid-state Camera Application



Pixellated Camera  
Lateral View



In spite of their initial expenses, solid-state cameras are finding use in specialized applications

Photos courtesy Jerome Gormley, Digirad, Inc

An improved spatial resolution due to the reduced light spread !!

Anger Camera  
Lateral View



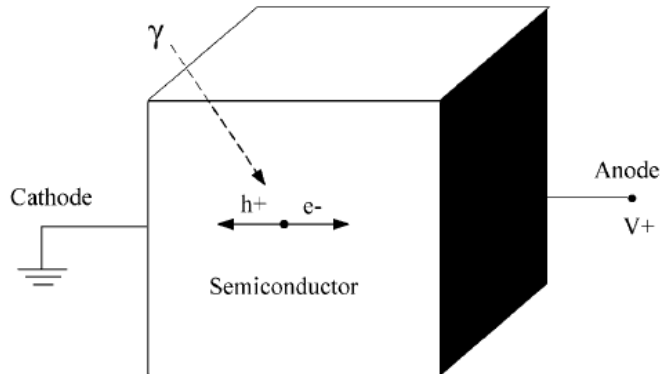
# Comparing HPGe and Room Temperature Semiconductor Materials

Detector Material	Z	$E_G$ (eV)	$E_{pair}$ (eV/eHP)	Density (g/cm <sup>3</sup> )	Resistivity @ 300K ( $\Omega \cdot \text{cm}$ )	$\mu\tau_{e/h}$ (cm <sup>2</sup> /V)	Knoop Hardness
Ge	32	0.66	2.9	5.33	50	>1/>1	
Si	14	1.12	3.6	2.33	$\sim 10^4$	>1/ $\sim 1$	1150
CdTe	48/52	1.4	4.4	6.2	$10^9$	$10^{-3}/10^{-4}$	45
CdZnTe	48/30/52	1.6	4.7	$\sim 6.2$	$10^{11}$	$10^{-2}/10^{-4}$	
HgI <sub>2</sub>	80/53	2.1	4.2	6.4	$10^{13}$	$10^{-2}/10^{-4}$	<10
GaAs	31/33	1.4	4.3	5.32	$10^8$	$10^{-5}/10^{-6}$	
Diamond	6	5	13	3.51	$>10^{13}$	$10^{-5}/10^{-5}$	10000
TlBr	81/35	2.7	5.9	7.56	$10^{11}$	$10^{-5}/10^{-6}$	
InP	49/15	1.4	4.2	4.78	$10^7$	$10^{-5}/10^{-5}$	

In semiconductor: total signal generated:  $\sim 22,700 \rightarrow$  much smaller statistical fluctuation compared with that for scintillator!!

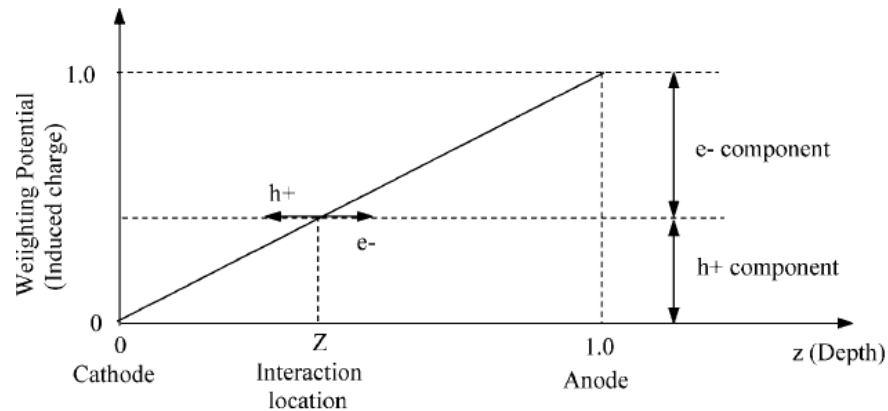
Further helped by the Fano factor (Please see the definition on page 115 and typical value for semiconductor on page 357, both on G. F. Knoll's text)

# Semiconductor Detector



The charge  $Q$  induced on an electrode by a moving point charge  $q$  are given by

$$Q(t) = -q \cdot \phi_0(\dot{x}(t))$$

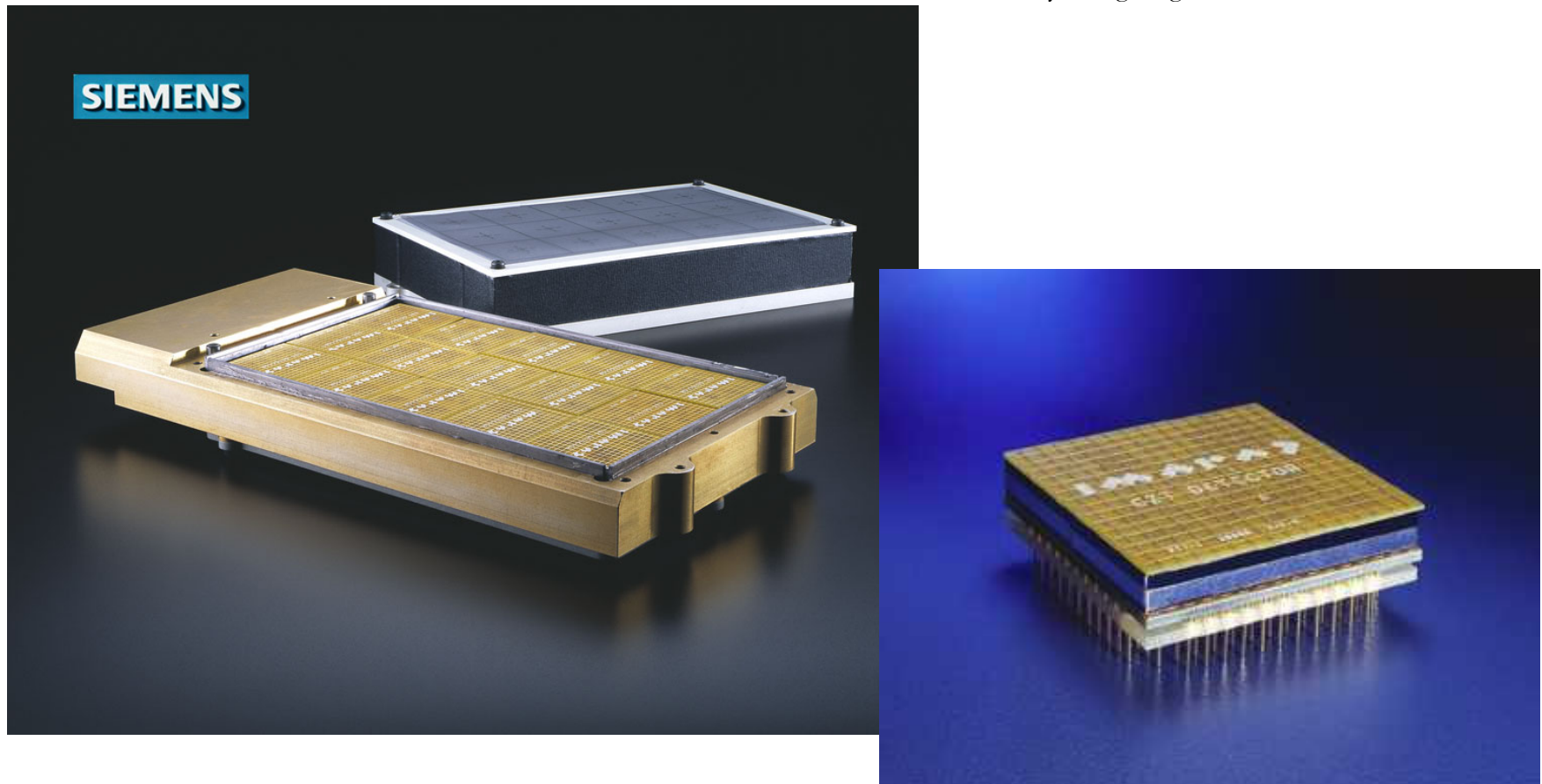


[1] W. Shockley, Currents to conductors induced by a moving point charge, J. Appl. Phys. 9 (1938) 635.

[2] S. Ramo, Currents induced by electron motion, Proceedings of the I.R.E., September 1939, p. 584.

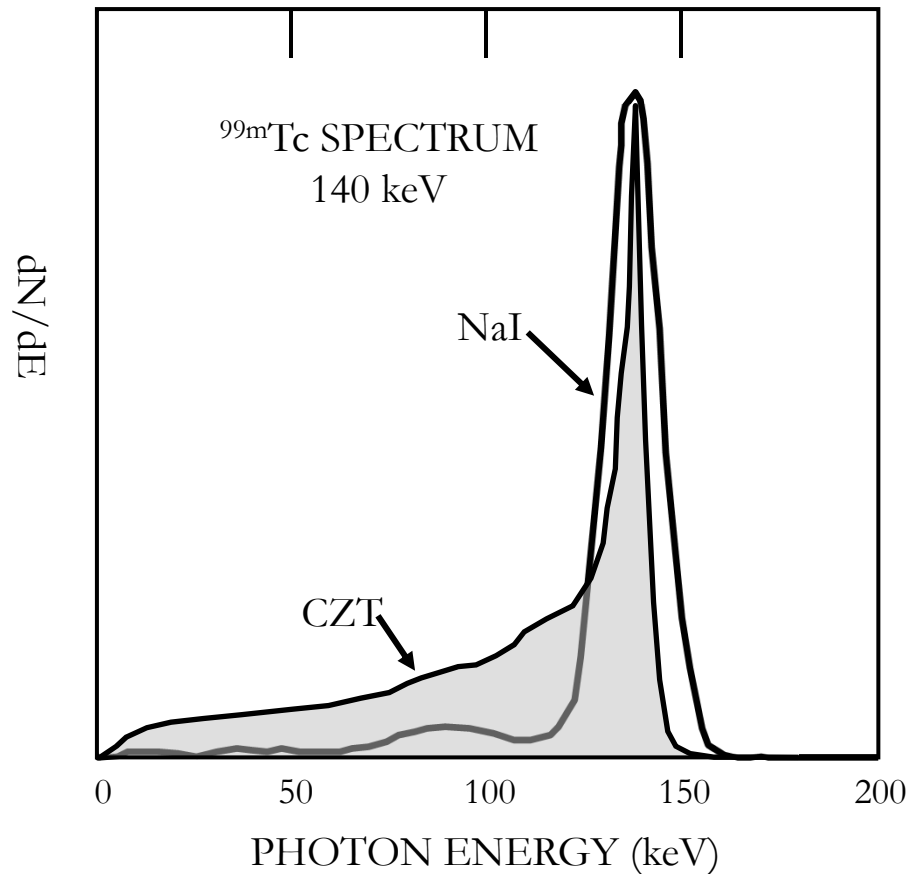
# SIEMENS CZT “CASSETTE” (12 cm x 20 cm)

Courtesy Doug Wagenaar, Siemens Medical Solutions



Works-in-progress prototype, not available as a product.

# Scintillation Crystal Properties



We are not quite there yet in terms of the achieved energy resolution. But the benefit in overall image quality is already significant!

$^{99m}\text{Tc}$  intrinsic (non-collimated) spectra obtained with CdZnTe (CZT) and NaI(Tl) detector systems. Note the low energy “tailing” of the CZT, and the 110 keV escape peak in the CZT spectrum.

Courtesy Doug Wagenaar, Siemens Medical Solutions

# NaI versus CZT Comparison

NaI



CZT



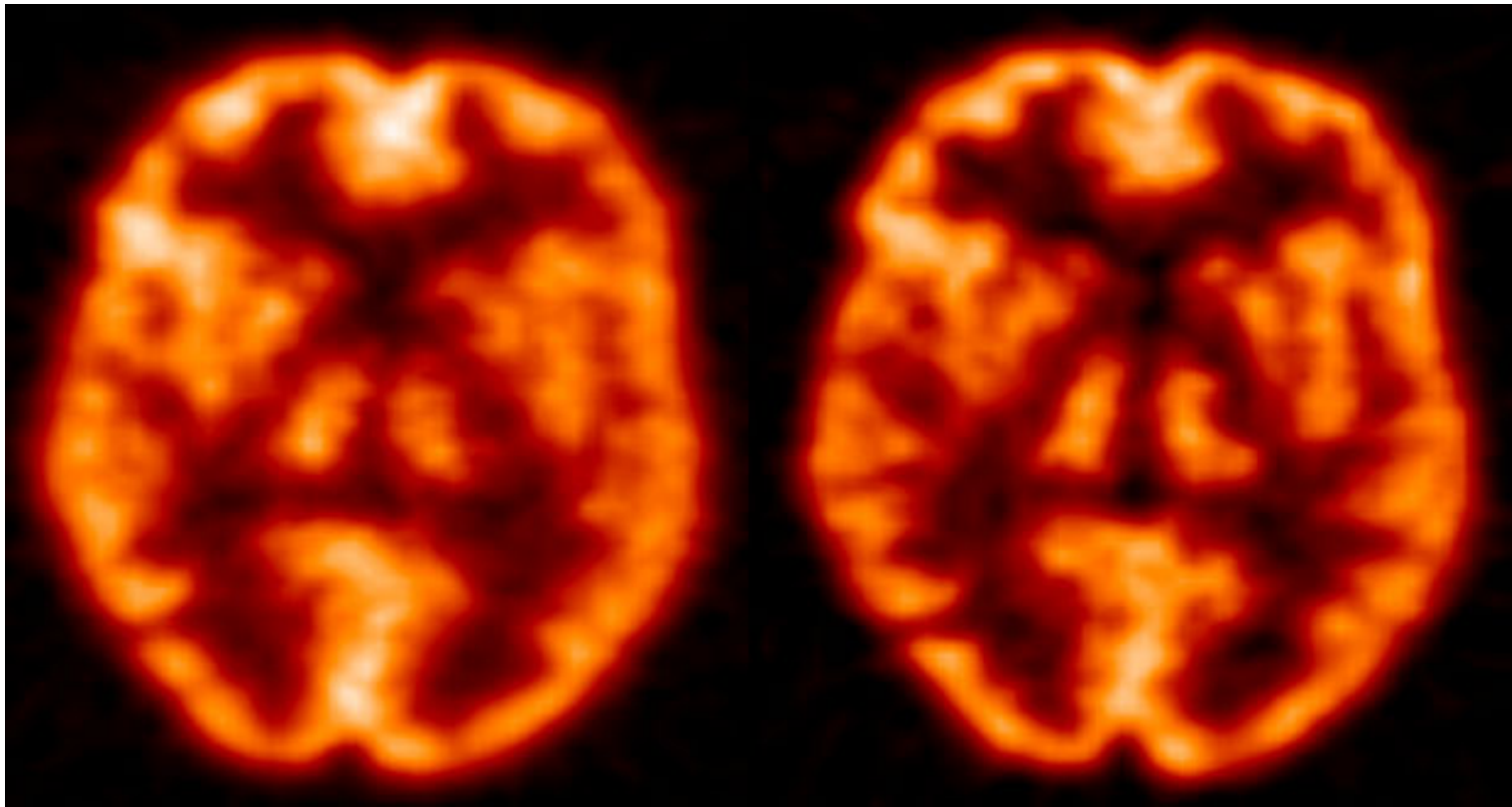
SIEMENS CZT CASSETTE

Courtesy Doug Wagenaar, Siemens Medical Solutions

# Brain Images

NaI

Mosaic CZT



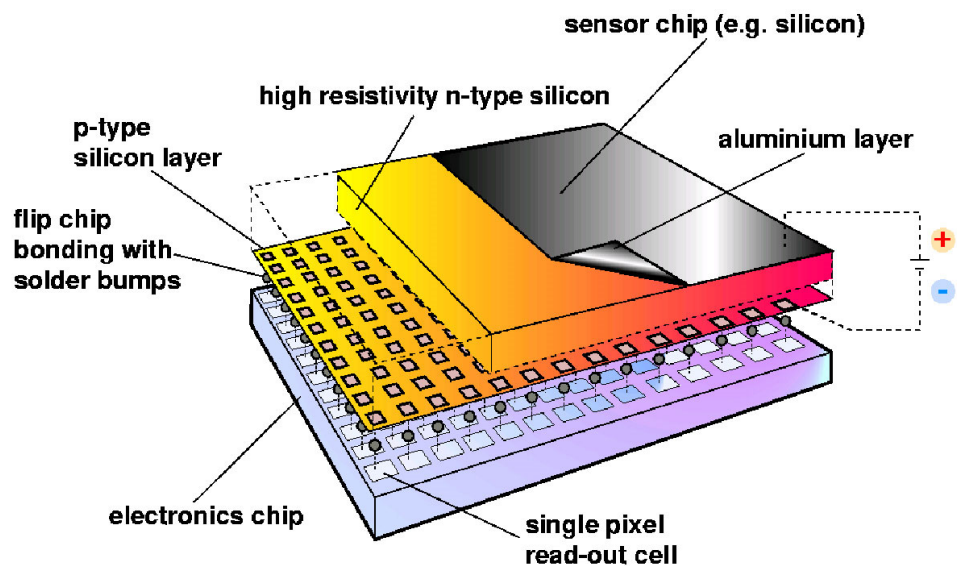
Improved Image Quality

# Small-Pixel Semiconductor Detectors

Is this the solution for future ultrahigh resolution nuclear imaging systems?

Not quite ...

- Energy resolution affected by incomplete charge collection.
- DOI resolution is either unavailable, or relatively poor.
- Timing information is limited by the slow charge drifting in semiconductor.
- Count rate capability MAY be limited by the complexity of the readout system.
- A single detector capable for both PET and SPECT is not available.

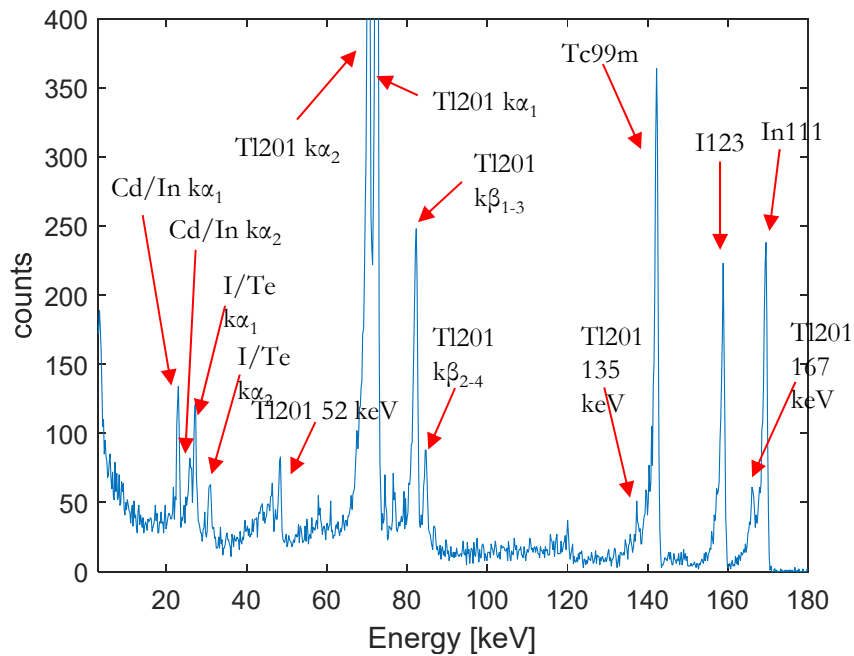


Medipix II hybrid pixel sensor

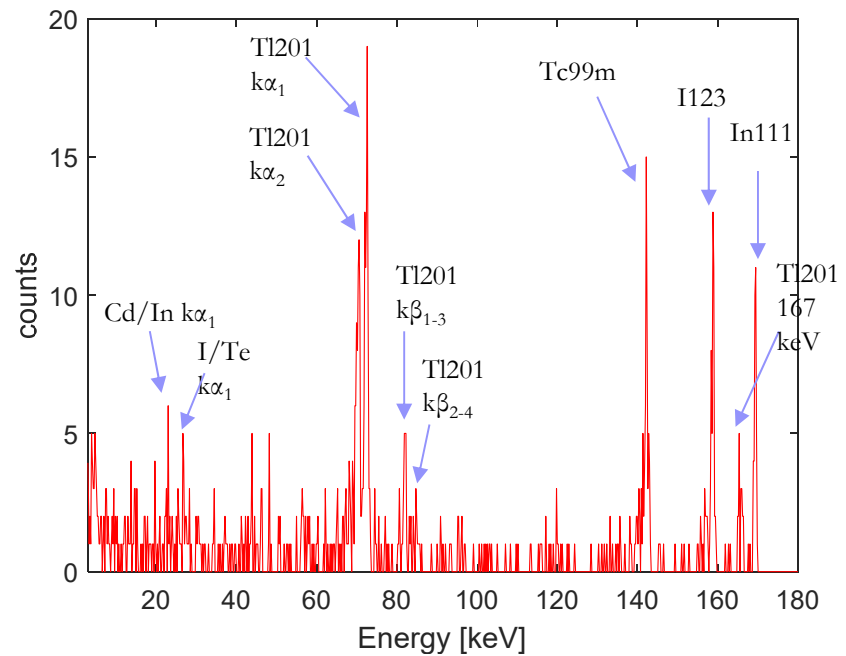
M. Campbell, V. Rosso, IEEE NSS-MIC 2004 Conference Record.

# 4 radioisotopes

0.1 mL each/0.25 mCi  
(Tc99m, Tl201, I123, In111)  
4 vials of 250 uL, parallel to set surface  
1 hr at 800 fps  
No Scattering media



Energy resolution obtained with all 6400 pixels on a 2 cm x 2 cm CdTe detector



Energy resolution obtained on a single pixel

# Controlled Charge Collection

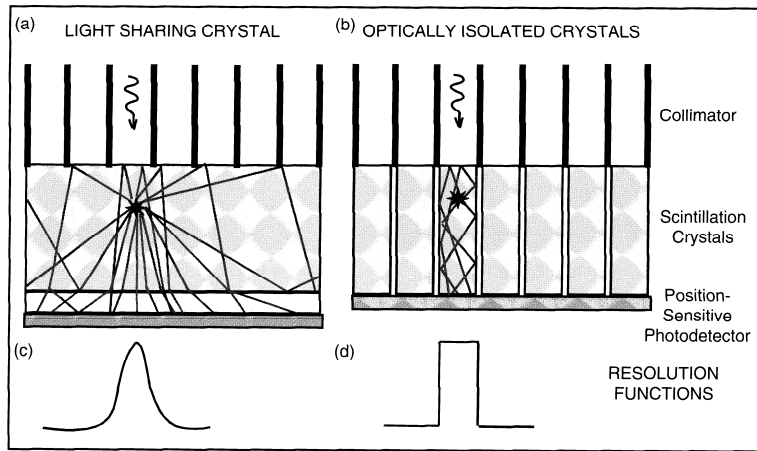
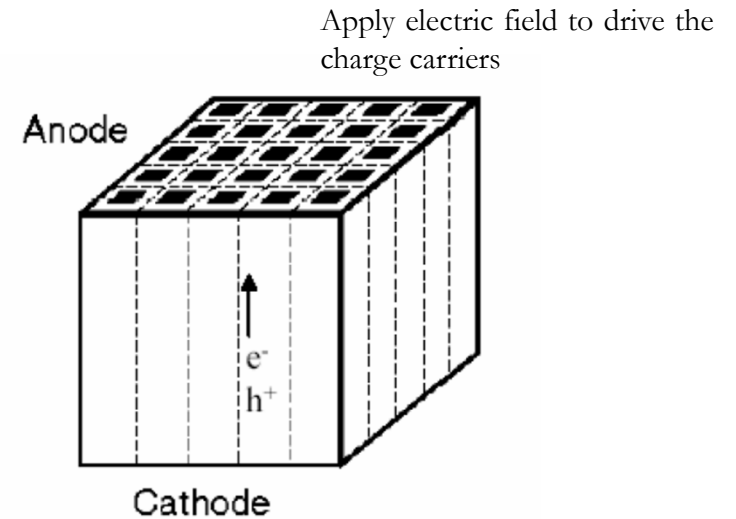


FIGURE 6 Schematic drawings of the light ray propagation for typical (a) single and (b) multiple scintillation crystal camera designs. For the pixellated design, scintillation light is confined to one crystal and focused on one spot of the photodetecting array. (c,d) Approximate shapes of the resulting theoretical intrinsic point spread functions for single-photon imaging.

Collection of visible photons in scintillator

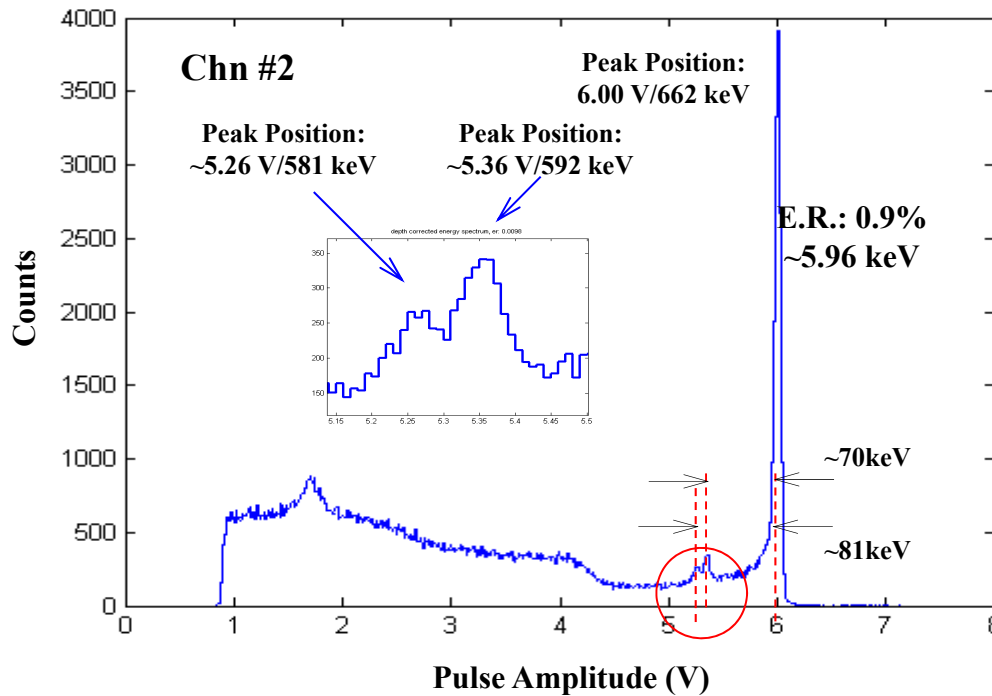


Collection of charge carriers in semiconductor

In semiconductor, electron and holes are driven by electric field.

Spatial spreading of the charge carriers can be better controlled, so that a better spatial resolution can be achieved.

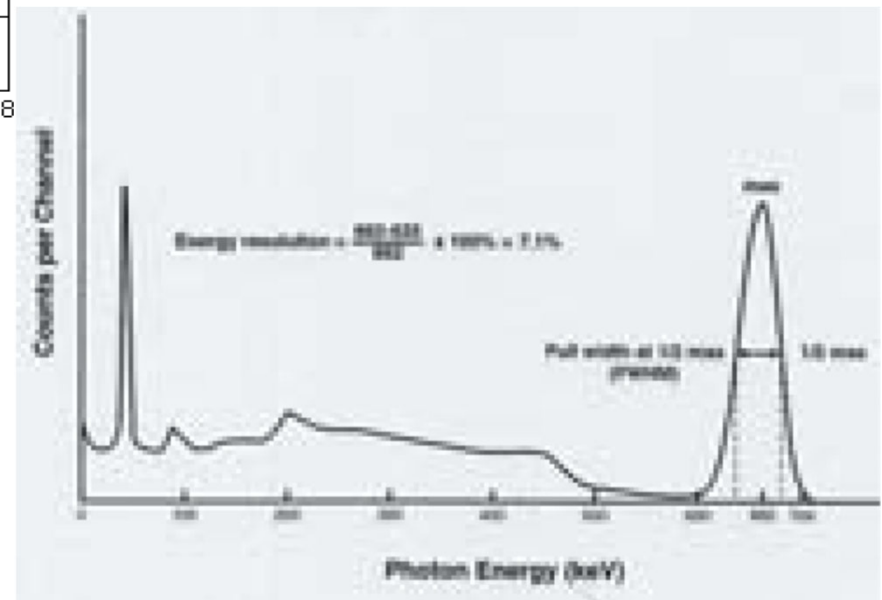
# A Typical Measured Energy Spectrum



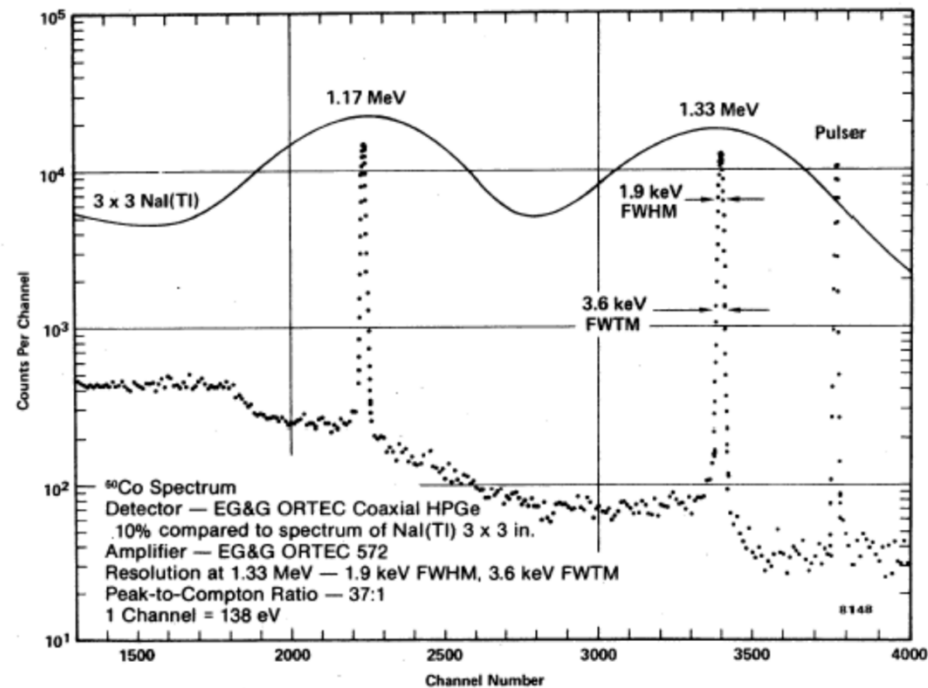
Typical energy spectrum from a 3 inch NaI(Tl) scintillation counter



Measured energy spectrum from HgI<sub>2</sub> semiconductor, 1mm thick, 1x1mm<sup>2</sup> pixels



# Comparing Co-60 Spectra Measured with NaI(Tl) and HPGe Detectors



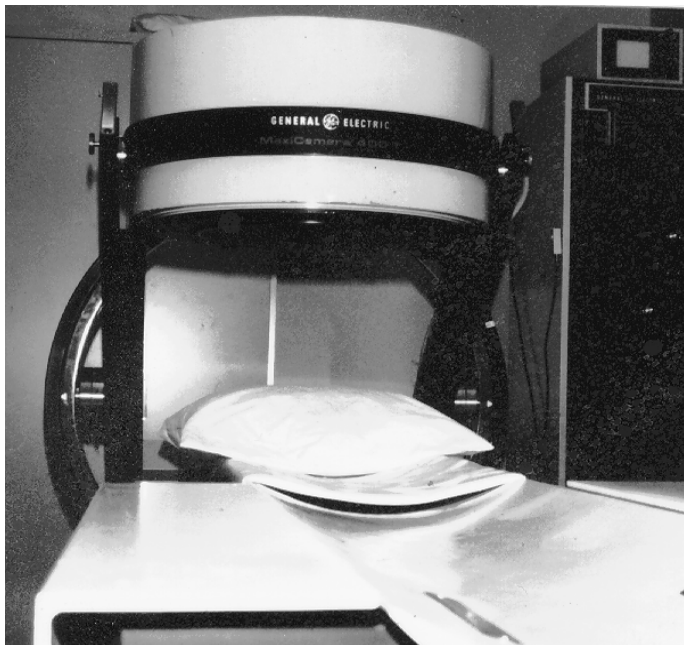
One of the major advantages of semiconductor detector is the improved energy resolution ..



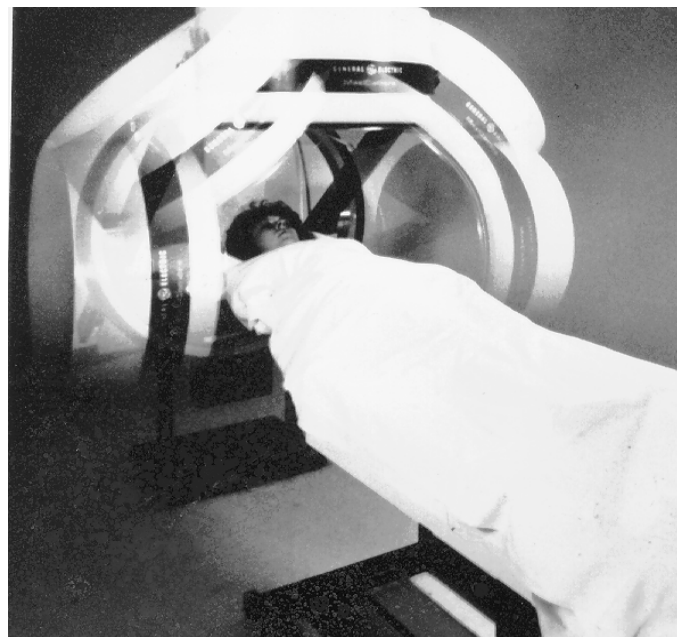
# Image Formation



# Early Clinical SPECT



The First Anger Camera



GE 400T Rotating Anger Camera (ca. 1981)

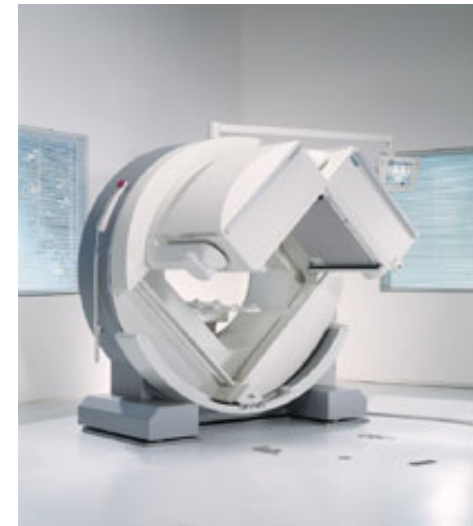
# Modern Clinical Systems



GE Millenium VG

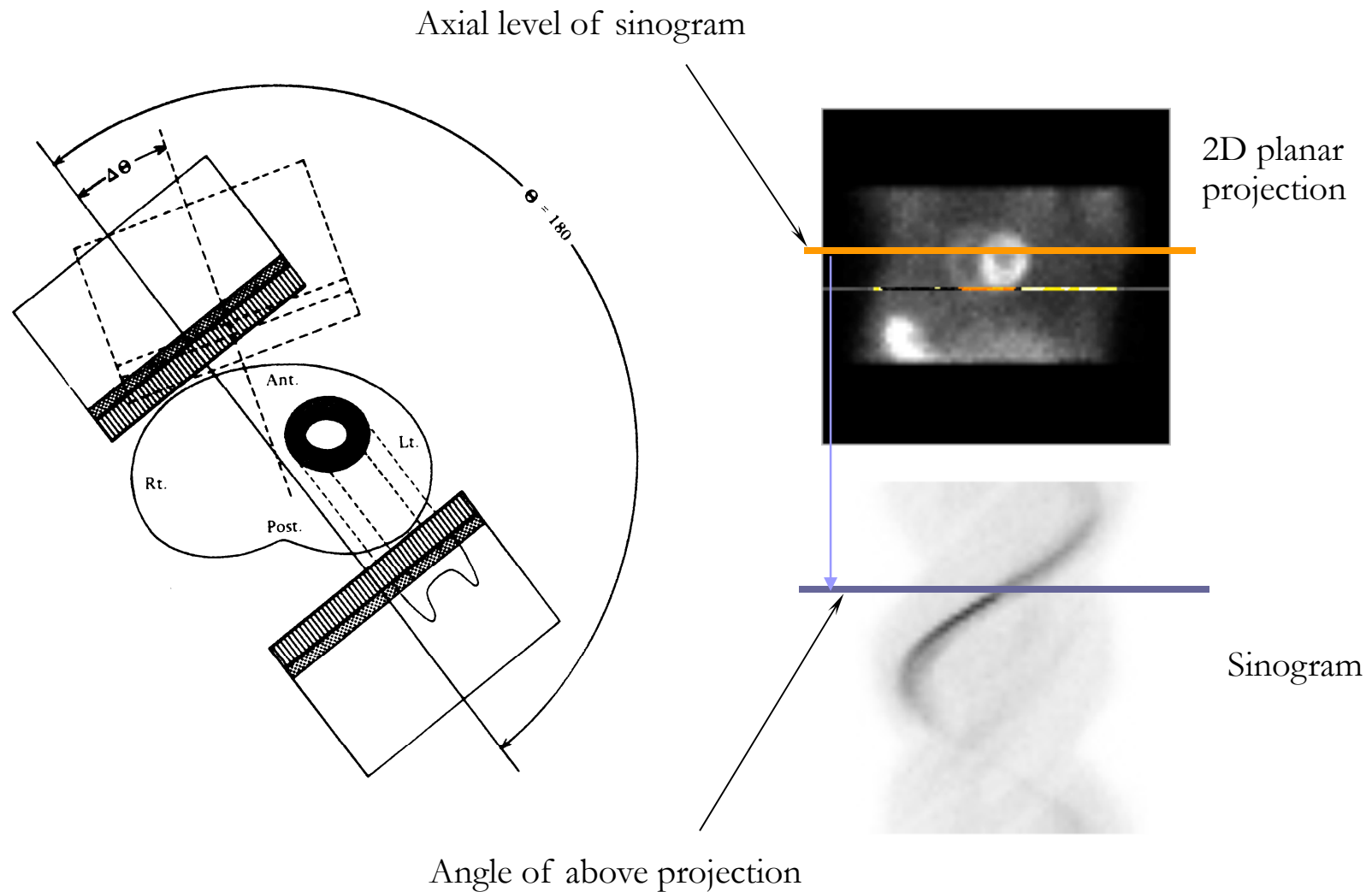


Philips Cardio 60



Siemens e.cam  
Variable Angle

# Basic SPECT – Projection Data

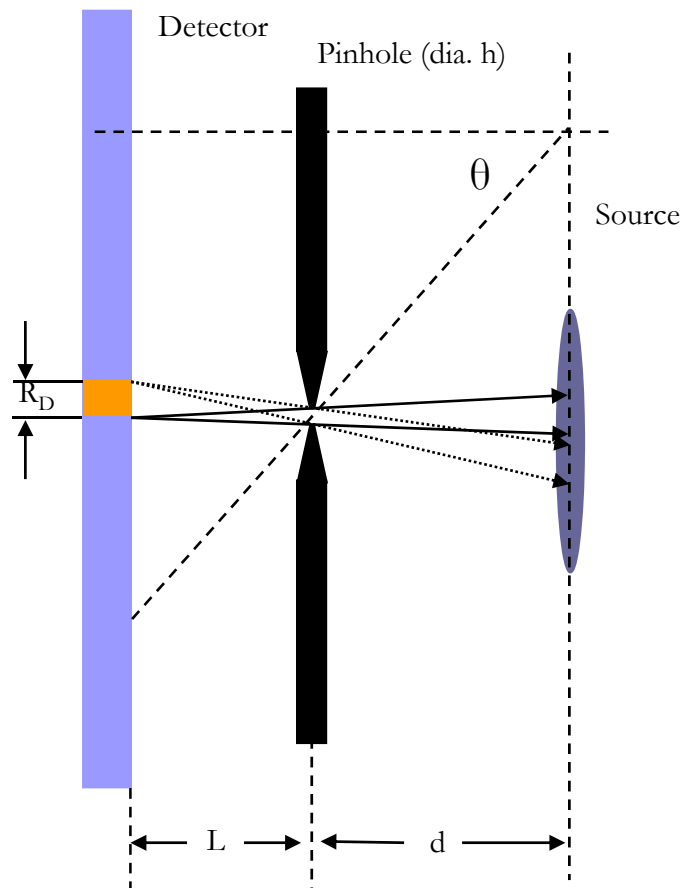




# Collimation Systems

- The collimation system is the heart of the SPECT instrument – it's the front-end and has the biggest impact on SNR
- Its function is to form an image by determining the direction along which gamma-rays propagate
- Ideally, a lens similar to that used for visible photon wavelengths would be used for high efficiency – not feasible at gamma-ray wavelengths
- Absorbing collimation typically used

# Pinhole Collimation



Intrinsic Resolution

$$R = h + \frac{h}{L} \times d$$

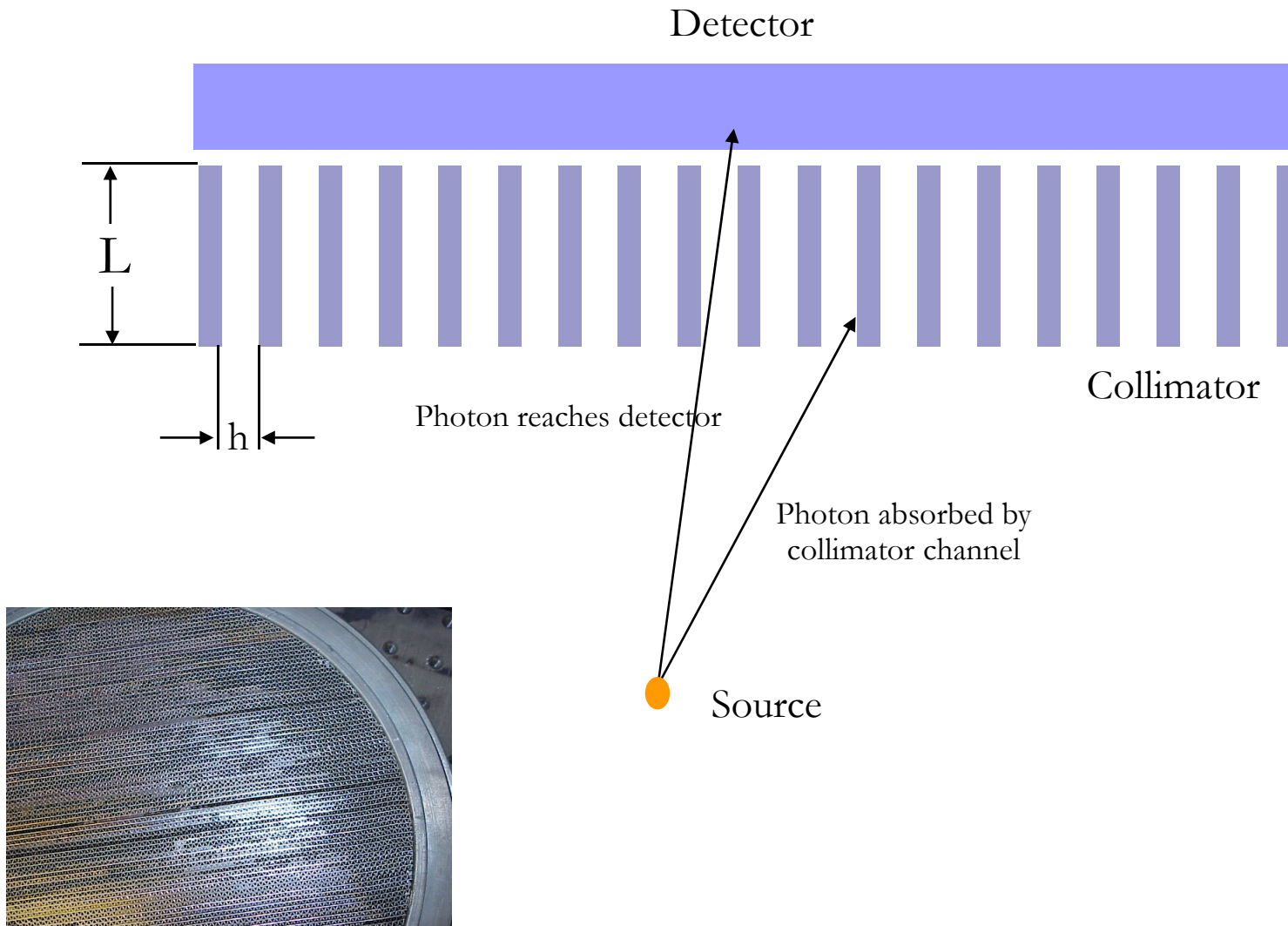
Efficiency

$$\eta < \frac{h^2}{16d^2} \cos^3 \theta$$

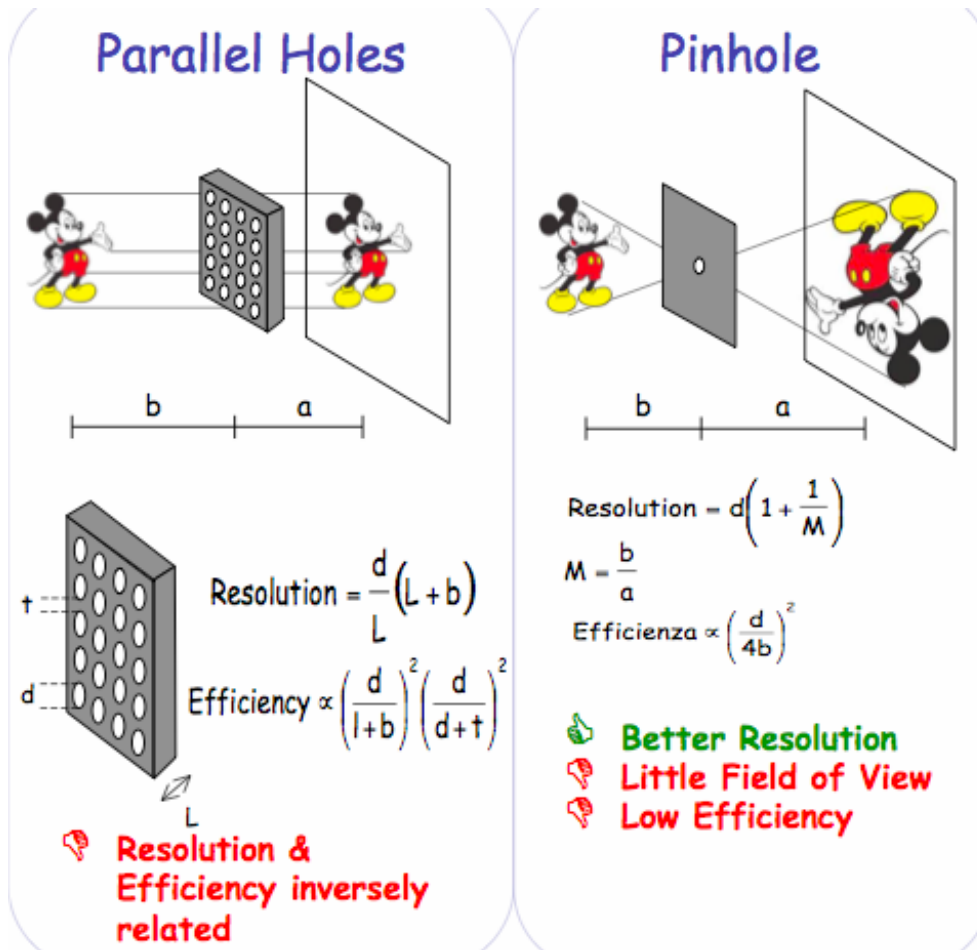
Combined Resolution

$$R_{\text{Total}} \approx \sqrt{\left( R^2 + \left( \frac{d}{L} \times R_D \right)^2 \right)}$$

# Parallel Hole Collimation



# How to Improve the Tradeoff between Spatial Resolution and Sensitivity?



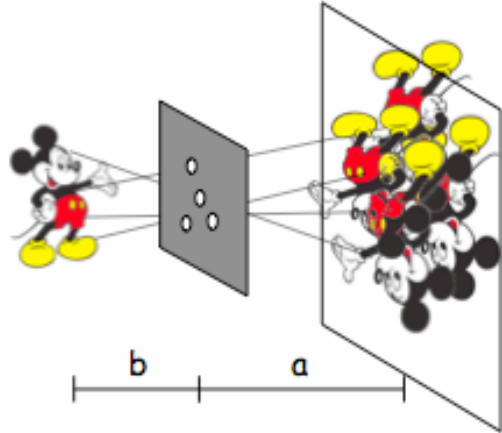
Better resolution →

- smaller hole diameter,
- better detector intrinsic resolution,
- smaller source to object distance.

Better sensitivity → Larger hole diameter

# How to Improve the Tradeoff between Spatial Resolution and Sensitivity?

**Coded Aperture**



Resolution =  $d \left( 1 + \frac{1}{M} \right)$

$M = \frac{b}{a}$

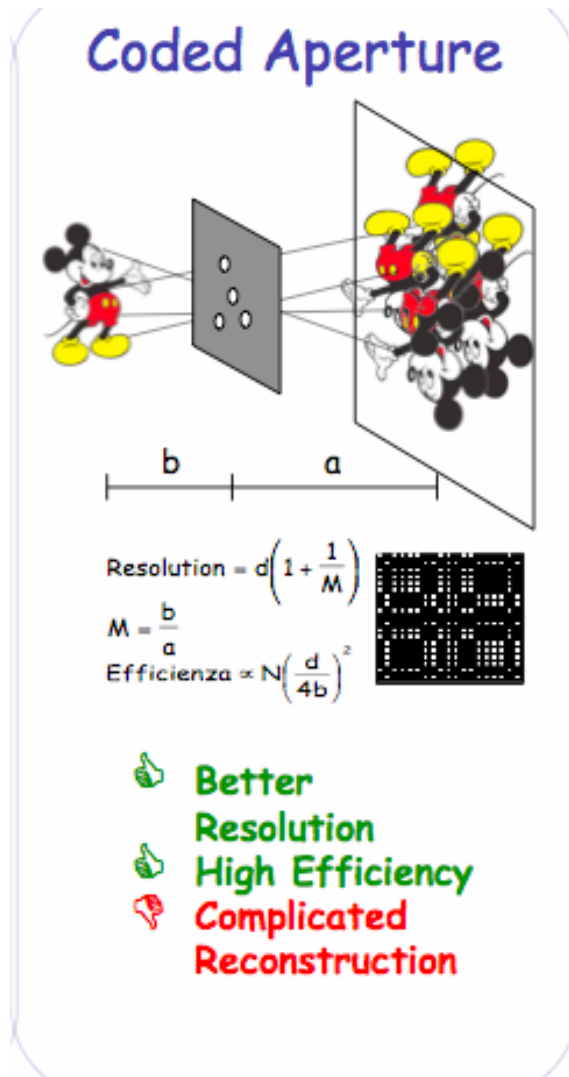
Efficienza  $\propto N \left( \frac{d}{4b} \right)^2$

- 👍 Better Resolution
- 👍 High Efficiency
- 👎 Complicated Reconstruction

What if we increase the open fraction to allow more photons to pass through ...

but split the total opening area into smaller pinholes ?

# How to Improve the Tradeoff between Spatial Resolution and Sensitivity?



The idea of **multiplexing** –

- Each detected photon no longer corresponds to a unique emission location in the 2-D source plane.
- Information content per detected photon is decreased.
- No of detected photons is increased.

# The Concept of Coded Aperture Imaging

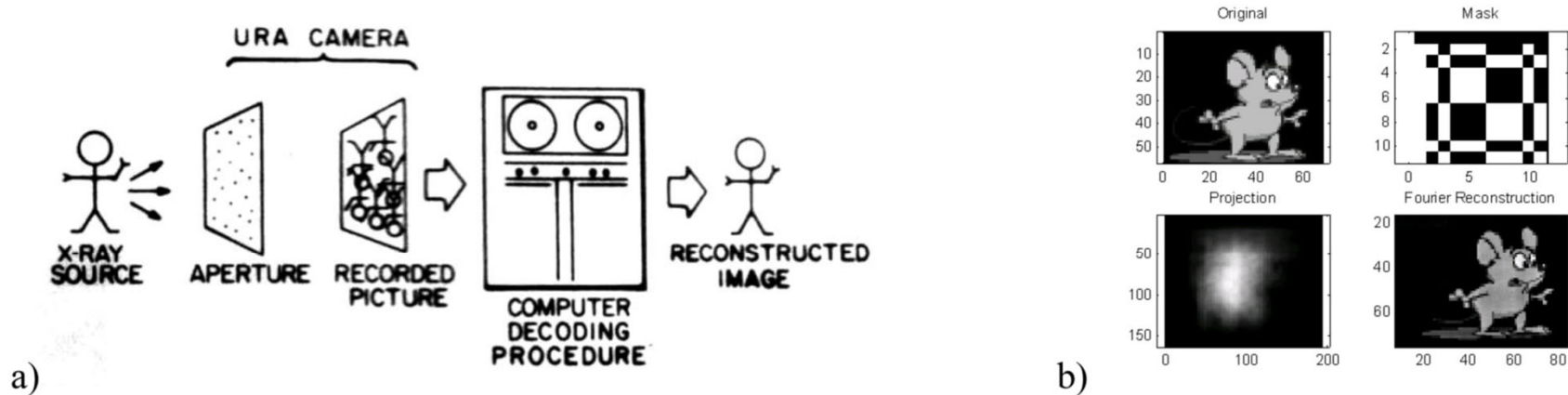


Figure 1.3: a) pictorial summary of a coded aperture camera concept (here indicated with a URA camera). Adapted from [6]. b) a sample of the process from the object, through the mask, to projection and reconstruction.

For a projection  $A$  from a point source, if there are decoding patterns  $G$  that gives:

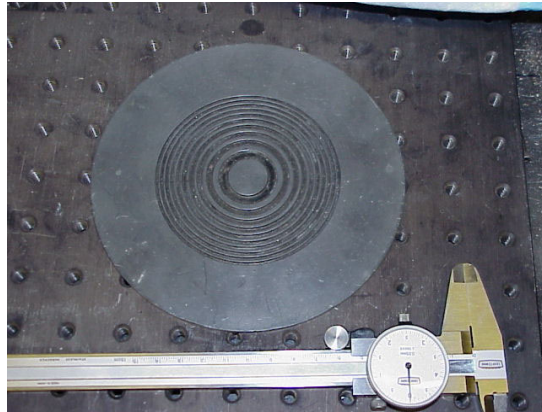
$$A \otimes G = \delta$$

Then for any projection  $R$  from an arbitrary source function  $O$ , the original source function  $O$  may be recovered by

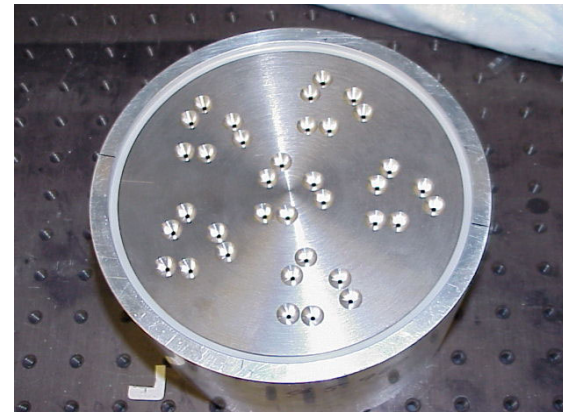
$$\hat{O} = R \otimes G, \text{ in fact}$$

$$\hat{O} = R \otimes G = (O \times A) \otimes G = O * (A \otimes G) = O * \text{PSF}$$

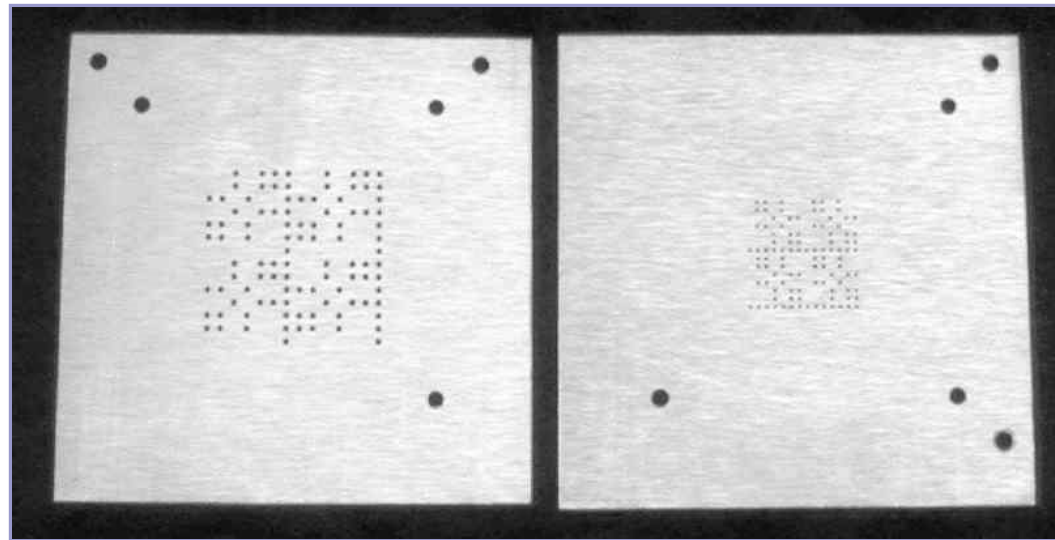
# Examples of Coded Apertures



Fresnel Zone-Plate



Multiple Pinhole Aperture



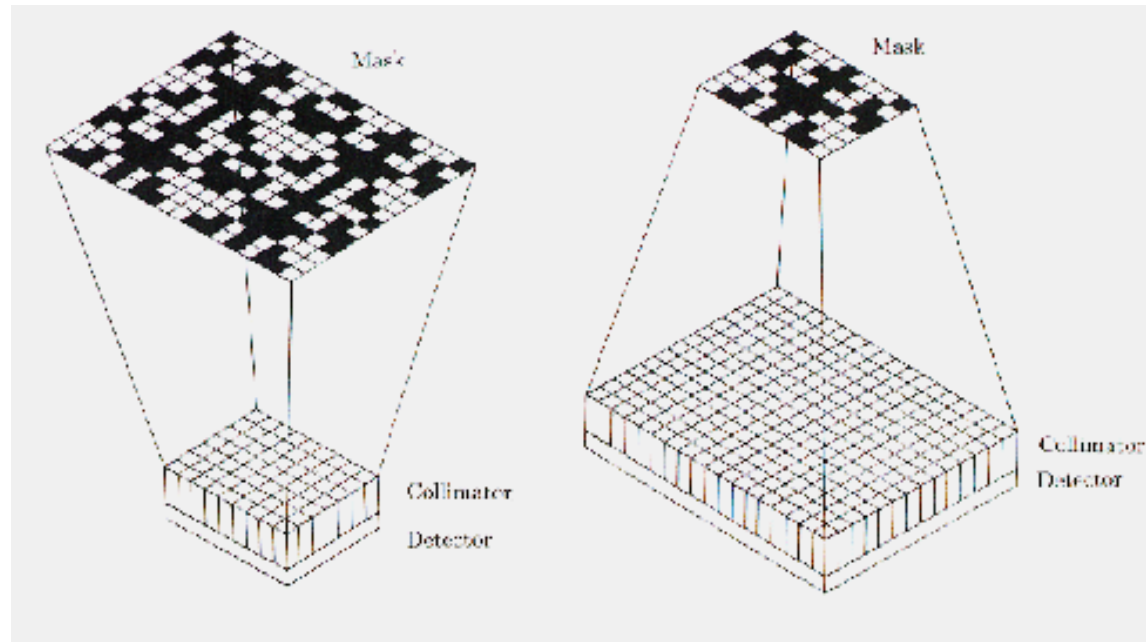
Uniformly Redundant Array Aperture, Accorsi et al, 2002



# Astronomical Application of Coded Aperture Imaging

- Gamma ray sources are normally point-like with very low or virtually no background.
- Sources are normally well separated from each other.
- Very low flux reaching the detector – sensitivity is very important for making quantitative conclusions.
- A wider FOV is normally required to survey a larger portion of the sky

# Typical Coded Aperture Imaging System



- Apertures that consists of transparent and opaque elements
- Open fraction as high as 50% ( $10^{-4} \sim 10^{-3}$  with pinhole or parallel hole collimators.)
- Position sensitive detector used to detect the “shadow” images projecting through the mask.

# Coded Aperture Imaging

Coded aperture is, from some sense, an multiple pinhole aperture with more openings ...

The way to reconstruct the image:

1. ML based method (optimum)
2. Cross-correlation – Computationally efficient, does not model detailed detector response, less optimum image quality (Please see literatures on NERS435 class website for details)

Coded aperture is the standard imaging technique in astrophysics application involving hard x-rays and gamma rays.

[http://astrophysics.gsfc.nasa.gov/cai/coded\\_inss.html](http://astrophysics.gsfc.nasa.gov/cai/coded_inss.html)

Capabilities (as designed)

Instrument/ Platform	PI/ country	Science <sup>2</sup>	Operat. period	Detector/ E. range (keV) E-resolution	Pattern <sup>2</sup> Config <sup>2</sup> Mask mat.	FOV <sup>2</sup> (degrees/ Ang. Res. (arcmin)	Det. Area (cm <sup>2</sup> )
Instruments flown							
SL 602 rocket	A. Willmore (U. B'ham) UK	GC	69	Film 0.6-1.6	FZP Fe	110 (HM) 7.6	205
MPC rocket	R. Blake (U. Chicago?) USA	Sun	72	Film 0.6-1.6	ORA Ni/Fe	0.25X0.25 (HM) 0.4	2
SL 1501 rocket	A. Willmore (U. B'ham) UK	GC	76	PSPC 2.2-10.2 18%@6 keV	URA Fe	3.8X3.8 (ZR) 2.5X21	450
TXC balloon	D. Cardini (?) ?	TR	81	PSPC 10-150 20%@60 keV	URA <sup>1D</sup> Pb	95X97 (ZR) 300X240	468
Burst camera / Gamma Cam balloon	H. Horstman (TESRE) Italy	GRB	83	NaI 30-300 20%@60 keV	ORA <sub>30</sub> Pb	119 (FC) 120	1200
HXT Tenma	M. Tsunemi (ISAS) Japan	ASM	83-84	PSPC 2-25 20%@6 keV	URA <sup>1D</sup> Fe/Cr	40X40 (HM) 60	140
DGT balloon	M. McConnell (UNH) USA	Crab,Cyg	84,88	BGO 160-9300 19%@662 keV	URA R/C Pb	15X23 (FC) 230	709
NRI Spacelab 2	A. Willmore (U. B'ham) UK	AGN, GC	85	PSPC 2-25 ~20%@6 keV	URA-p R/C Fe	3.2X3.2 (HM) 3,12	1024
COMIS-TTM Kvant-Mir	A. Brinkman (SRON) Netherlands & UK	transients gal. ridge GC	87-99	PSPC 2-30 18%@6 keV	URA-p R/S Fe/Au	8X8 (HM) 2	655
GRIP balloon	T. Prince (CalTech) USA	Crab, GC	88,89, 93,95	NaI 30-10000 23%@60 keV	HURA H/C Pb/Sn	14 (HM) 66	645
ZEBRA) balloon	G. Villa (TesRe) Italy	AGN, Crab, GC	89	NaI 150-10000 12%@661 keV	URA W	7X9 (FC) 60	2500
MIXE balloon	B. Ramsey (MSFC) USA	Crab,Cyg,AGN	89,93,97	MicroStrip 25-100 6%@60 keV	URA R/C W	1.8X1.8 (HM) 6.9	784
SIGMA Granat	J. Paul (CNES) France	GC, XB	89-99	NaI 30-1500 16%@60 keV	URA-h R/C W	11X11 (HM) 13	5000
ART-P Granat	R. Sunyaev (IKI) Russia	GC	89-93	PSPC 2-30 22%@6 keV	URA-h R/S Cu	1.8X1.8 (HM) 6	655
(Gamma-L) Gamma	V. Akimov? (IKI) SU	GC, Sun	90-92	Spark 35-1300 16%@60 keV	URA <sup>1D</sup> W	24 (HM) 20	1500
(URA) STS 39	E. Fennimore (LANL) USA	GC, Cen X-3	91	HP-GSPC 2-70 15%@6 keV	URA H/C W	4.5 (HM) 4	1000
EXITE-2 balloon	J. Grindlay (Harvard) USA	GC	93	NaI 20-600 18%@60 keV	URA R/C Pb/Sn/Cu	4.7X4.7 (HM) 23	1600
TIMAX balloon	J. Braga (INPE) Brazil	GC	93	NaI 30-100 25%@60 keV	URA R/M/A Pb-Cu	12X8.5 (ZR) 120	400
SAGE balloon	G. Skinner (U B'ham) UK	Crab	93	Ge 20-1500 ~0.5%	ORA Pb	16X4 (FC) 60	20

And many more ...

# An Typical Emission Tomography System Described in Matrix Form

The response function of the imaging system for an impulse signal at a given source location – The Impulse Response Function  $h_i$

$$\begin{pmatrix} g_1 \\ g_2 \\ g_3 \\ \vdots \\ g_M \end{pmatrix} = \begin{pmatrix} p_{11} & p_{12} & p_{13} & \dots & p_{1N} \\ p_{21} & p_{22} & p_{23} & \dots & p_{2N} \\ p_{31} & p_{32} & p_{33} & \dots & p_{3N} \\ \vdots & \vdots & \vdots & \ddots & \vdots \\ p_{M1} & p_{M2} & p_{M3} & \dots & p_{MN} \end{pmatrix} \begin{pmatrix} f_1 \\ f_2 \\ f_3 \\ \vdots \\ f_N \end{pmatrix}$$

No. of counts observed on a given detector pixel

$p_{mn}$ : the probability of a gamma ray generated at source pixel  $m$  being detected by detector pixel  $n$ .

$f_n$ : No. of gamma rays generated in a given source pixel

# Image Formation with Coded Apertures

Once the overlapping projection data is acquired, the underlying image of the source object can be recovered using the many reconstruction techniques, such as the ML based iterative approach

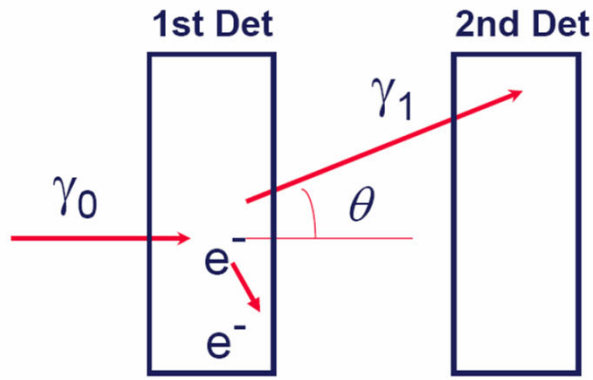
So the ML reconstruction for Poisson distributed data is

$$\hat{\mathbf{f}}_{ML} = \arg \max_{\mathbf{f}} l(\mathbf{f}, \mathbf{g}) = \arg \max_{\mathbf{f}} \left[ \sum_{m=1}^M (g_m \log \bar{g}_m - \bar{g}_m - \log g_m!) \right]$$

since  $g_m$  is not function of  $\mathbf{f}$ , we get

$$\hat{\mathbf{f}}_{ML} = \arg \max_{\mathbf{f}} l(\mathbf{f}, \mathbf{g}) = \arg \max_{\mathbf{f}} \left[ \sum_{m=1}^M (g_m \log \bar{g}_m - \bar{g}_m) \right]$$

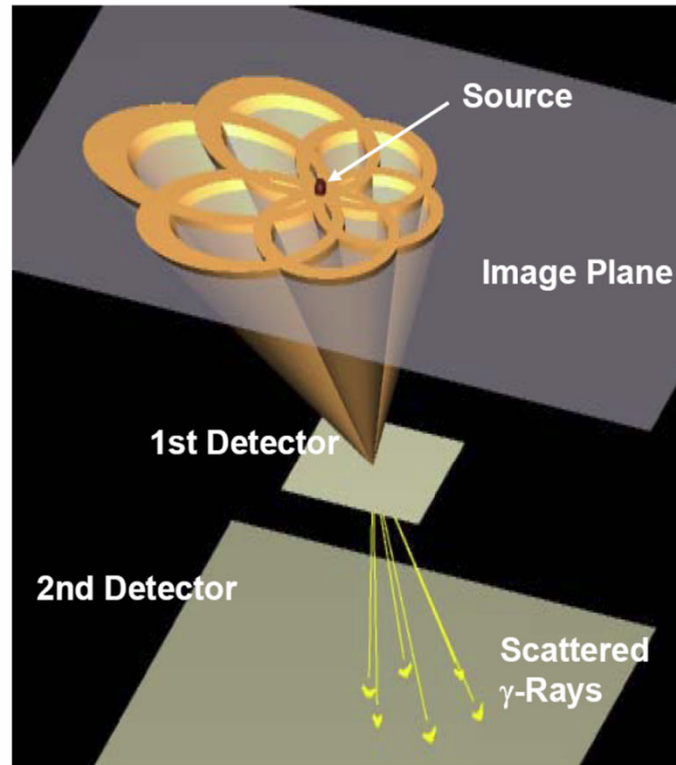
# Electronic Collimation Compton Camera



$$\frac{1}{E_1} - \frac{1}{E_0} = \frac{1}{511\text{keV}} (1 - \cos\theta)$$

$E_0$ : incident photon energy  
 $E_1$ : scattered photon energy  
 $\theta$ : scattering angle

1st det: solid state detector  
 2nd det: scintillation detector



Courtesy of Neal Clinthorne, U. Michigan.

# Energy Transfer in Compton Scattering

If we assuming the electron is free and at rest, the scattered gamma ray has an energy

$$hv' = \frac{hv}{1 + \frac{hv}{m_0c^2}(1 - \cos(\theta))},$$

Initial photon energy,  $v$ : photon frequency,  
 $h = 6.62607015 \times 10^{-34}$  meter · kilogram/second, (Planck' s constant)

mass of electron  $m_0c^2$  Scattering angle  $\theta$

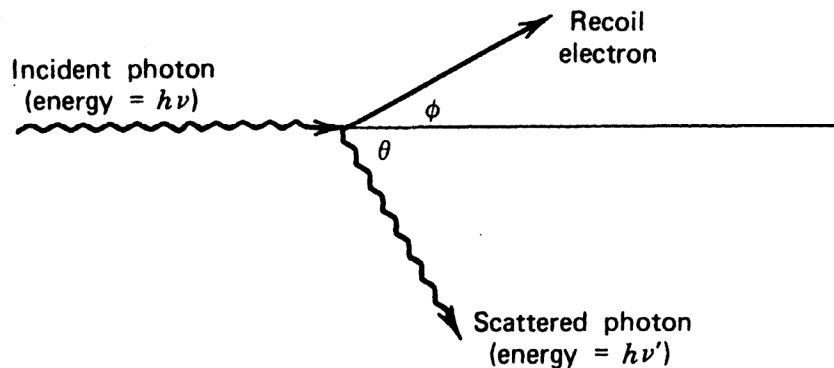
and the photon transfers part of its energy to the electron (assumed to be at rest), which is known as a recoil electron. Its energy is simply

$$E_{recoil} = hv - hv' = hv - \frac{hv}{1 + \frac{hv}{m_0c^2}(1 - \cos(\theta))}$$

The one-to-one relationship between scattering angle and energy loss!!

# Derivation of the Relation Between Scattering Angle and Energy Loss

The relation between energy the scattering angle and energy transfer can be derived based on the conservation of energy and momentum:



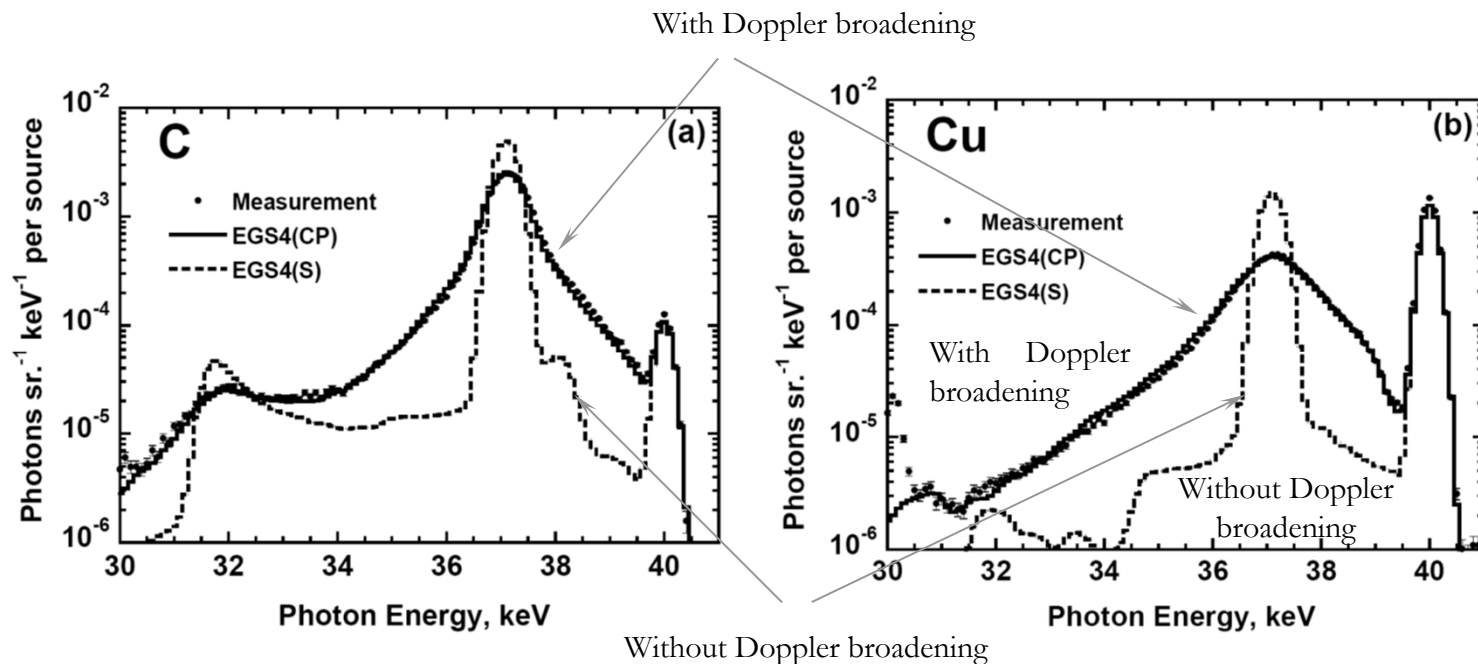
$$\vec{p}_{h\nu} + \vec{p}_e = \vec{p}_{h\nu'} + \vec{p}_{e'}$$

$$E_{h\nu} + E_e = E_{h\nu'} + E_{e'}$$

Are those terms truly zero?

# Compton Scattering with Non-stationary Electrons – Doppler Broadening

Comparison of the photon spectra scattered by C and Cu samples.  $E_{\text{hv}}=40\text{keV}$ ,  
 $\theta=90$  degrees

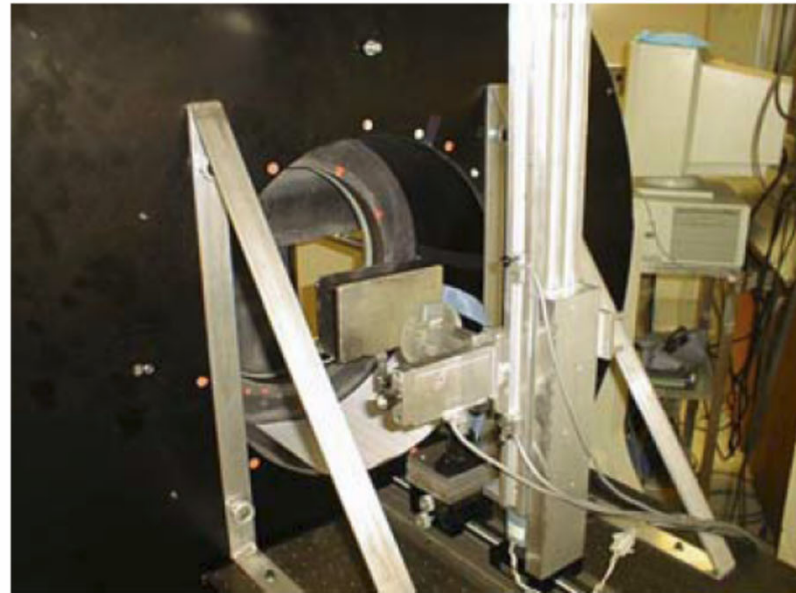


The Doppler broadening is stronger in Cu than in C because Cu electrons have greater bonding energies.

# Electronic Collimation



***Silicon pad first detector***



***Compton camera***

Courtesy of Neal Clinthorne, U. Michigan.

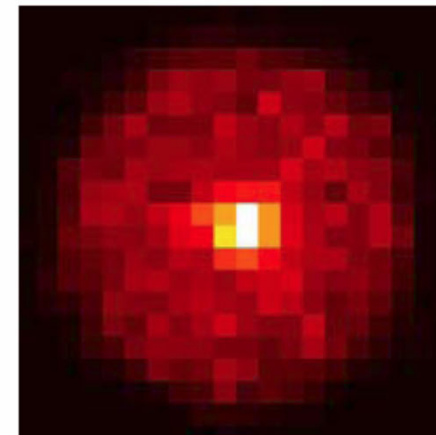
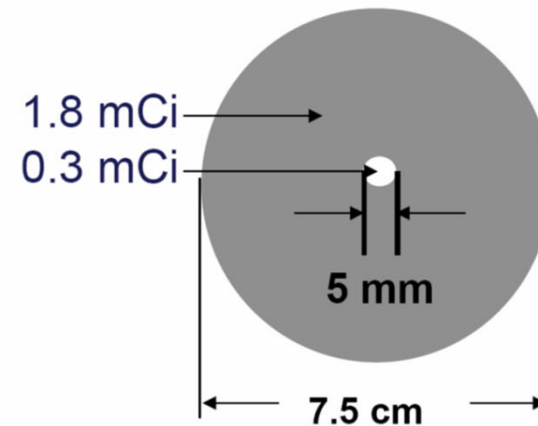
# Electronic Collimation

## Advantages

- *Spatial resolution and efficiency are more decoupled than with absorbing collimation – very high efficiency*
- *Performance improves dramatically with increasing energy – high resolution*

## Challenges

- *Very low noise required for first detector (~1 keV or less at 140 keV)*
- *System is electronically complex*
- *Image reconstruction is computationally challenging*

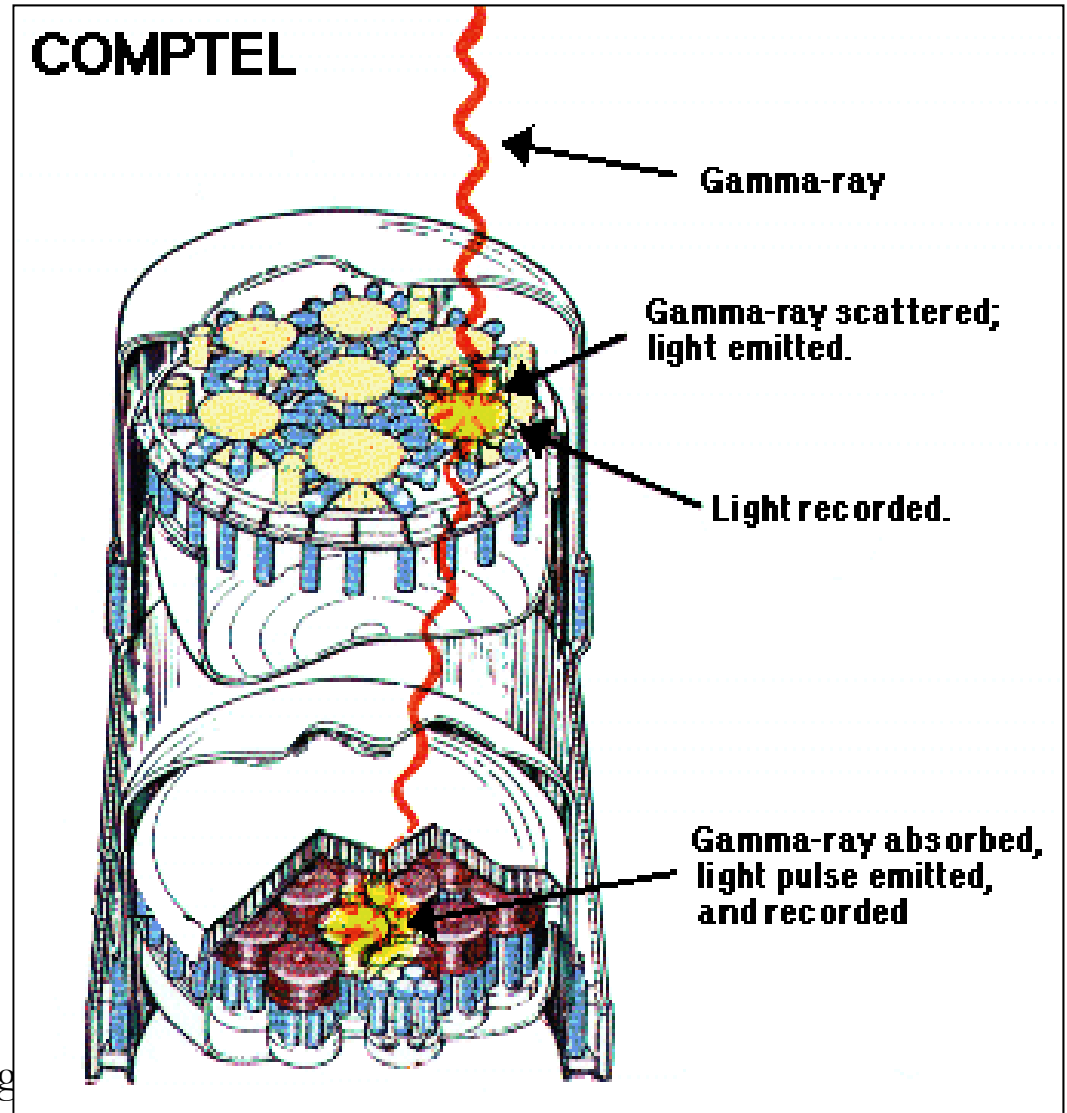


*Reconstruction of I-131 phantom*

Courtesy of Neal Clinthorne, U. Michigan.

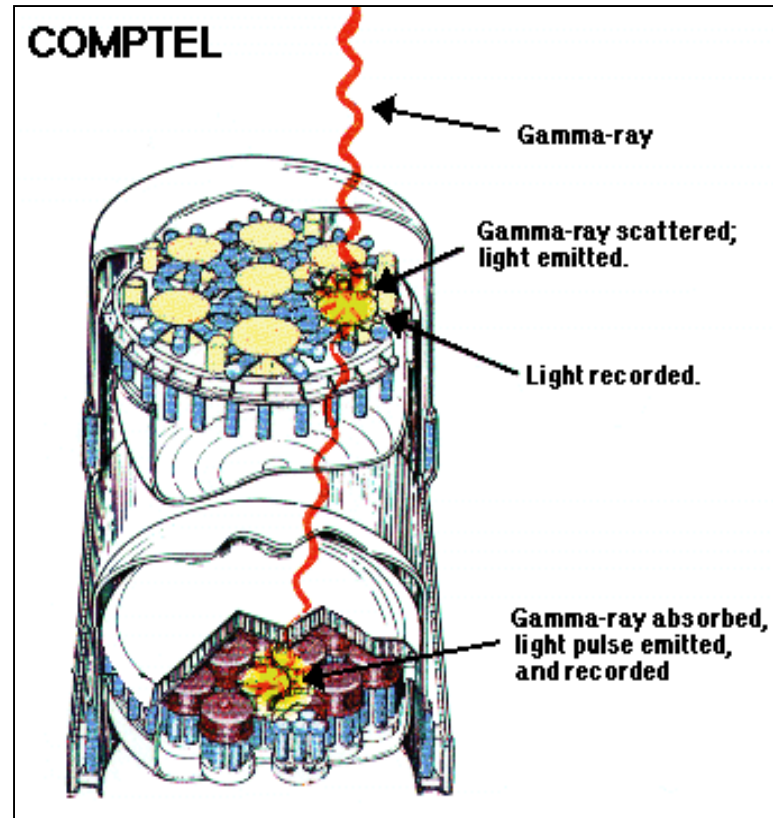
# The Comptel Observatory

- Compton telescopes are two-level instruments.
- Typically sensitive to photons between 300 eV and 30 MeV.
- Top level = photon Compton scatters in liquid scintillator.
- Bottom level = Scattered photon travels down and is absorbed by crystal scintillator.
- PMTs triggered on both levels.



Courtesy of Neal Clinthorne, U. Michigan

# The Comptel Observatory

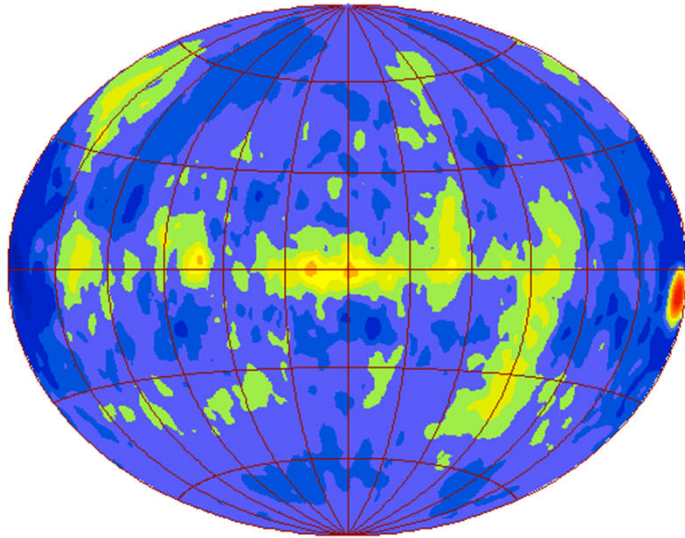


The Compton Gamma Ray Observatory was the second of NASA's Great Observatories. Compton, at 17 tons, was the heaviest astrophysical payload ever flown at the time of its launch on April 5, 1991 aboard the space shuttle Atlantis. Compton was safely deorbited and re-entered the Earth's atmosphere on June 4, 2000.



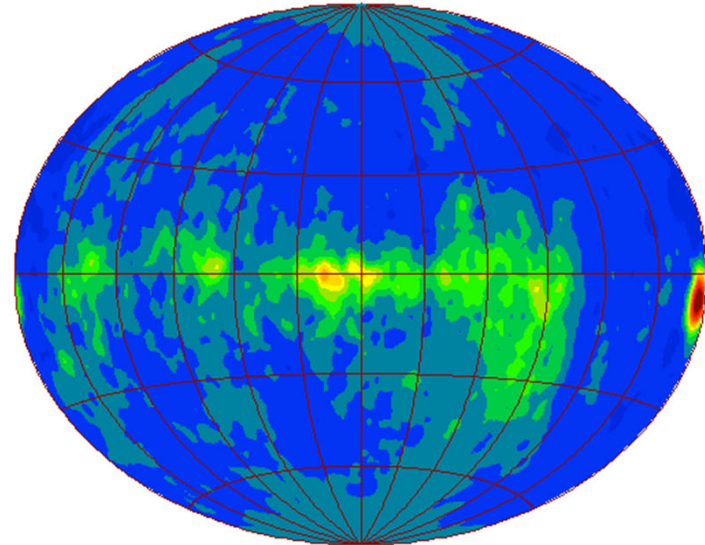
Comptel All-Sky Map

Phase 1+2+3 1-3MeV



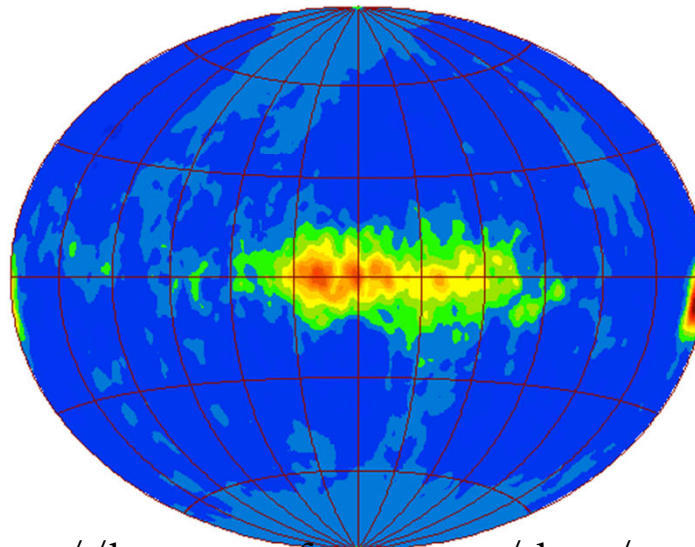
Comptel All-Sky Map

Phase 1+2+3 3-10MeV



Comptel All-sky map

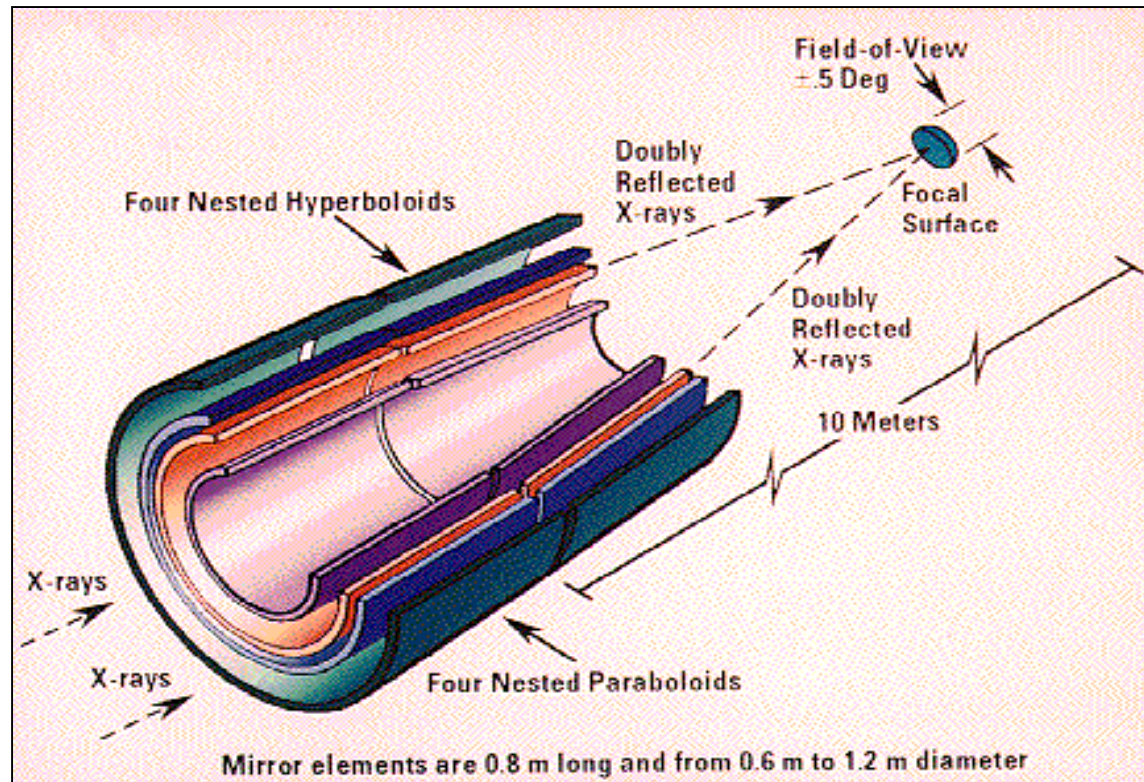
Phase 1+2+3 10-30MeV



<http://heasarc.gsfc.nasa.gov/docs/cgro/comptel/allsky.html>

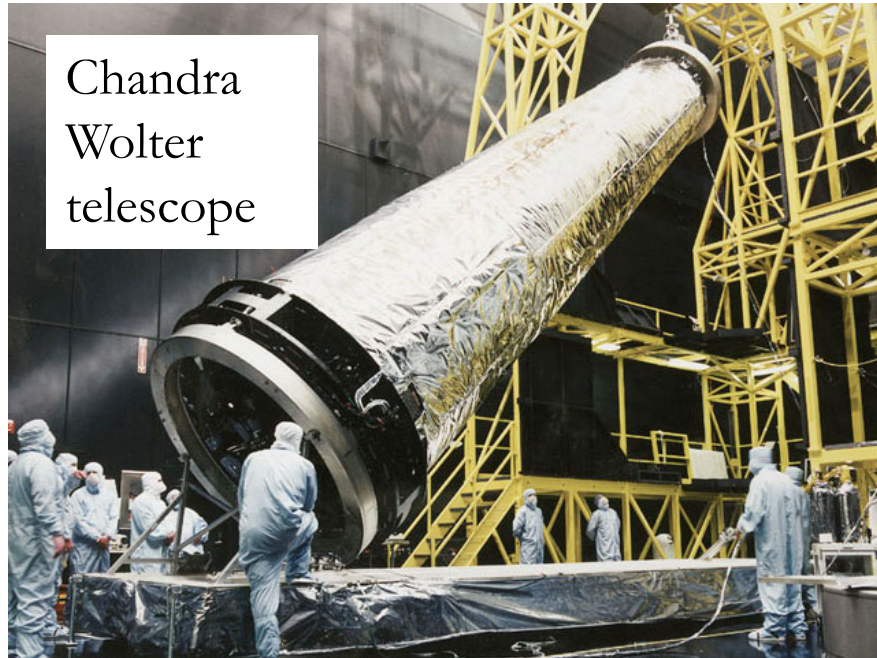
# Grazing Incidence Telescope

Uses fact that x-rays and gamma rays at very short wavelengths behave like ordinary light rays if they strike surfaces at a shallow enough angle.



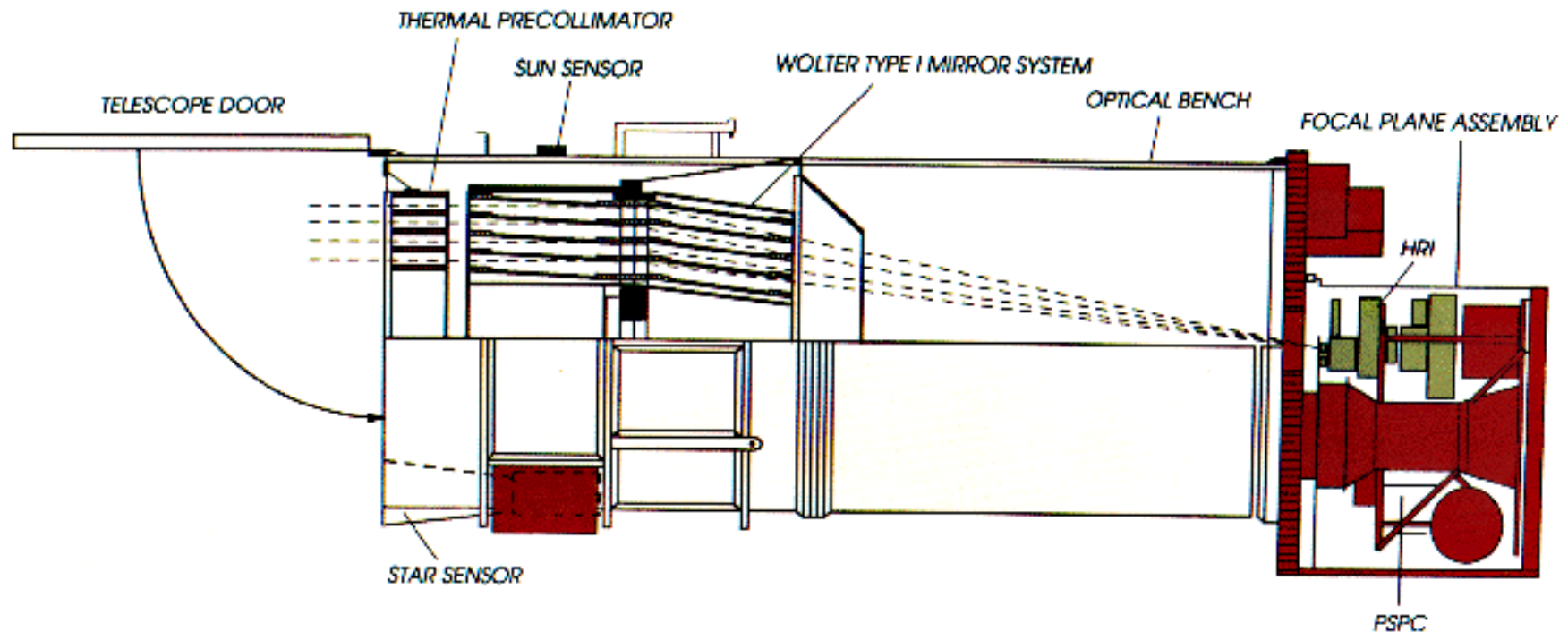
Only work if angle of reflection is very low (typically 10 arc-minutes to 2 degrees).

# The Chandra X-ray Observatory



# The ROSAT X-ray Observatory

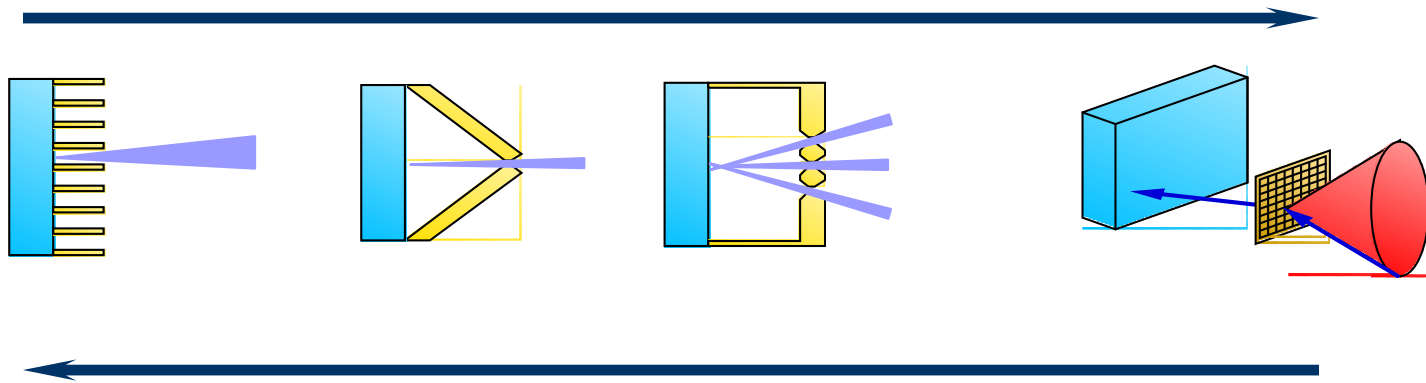
ROSAT (1990-1999) the ROentgen SATellite, was an X-ray observatory designed to make an all-sky survey in soft x-rays (0.1 keV-2 keV). Its sensitivity to X-rays was over 1000 times greater than Uhuru. The X-ray mirror assembly was a grazing incidence four-fold nested Wolter I telescope with an 84 cm diameter aperture.



# Electronic Collimation

Why electronic collimation?

Each detector element is allowed to see greater source volume →  
high sensitivity



Information content per detected photon is decreasing → the  
benefit depends on the particular source.



# Single Photon Emission Computed Tomography

## SPECT

Each projection view is 2-Dimensional → true 3-Dimensional imaging technique (cf. X-ray CT)

Spatial resolution of 10~15mm with 1 rotating camera

Clinical applications :

- Detection of tumor

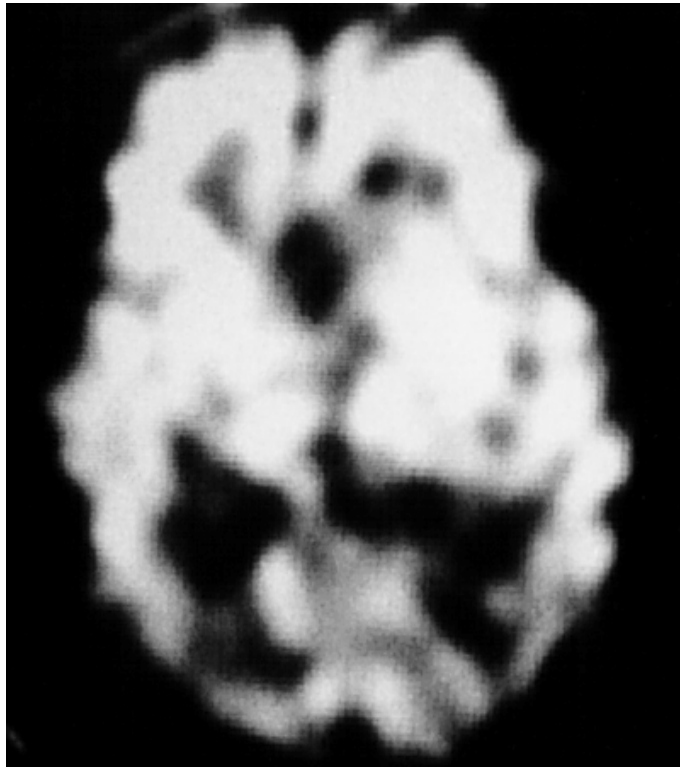
- Assessing myocardial infarction

- Blood perfusion in the brain

Typical imaging time : ~30min with 1 camera

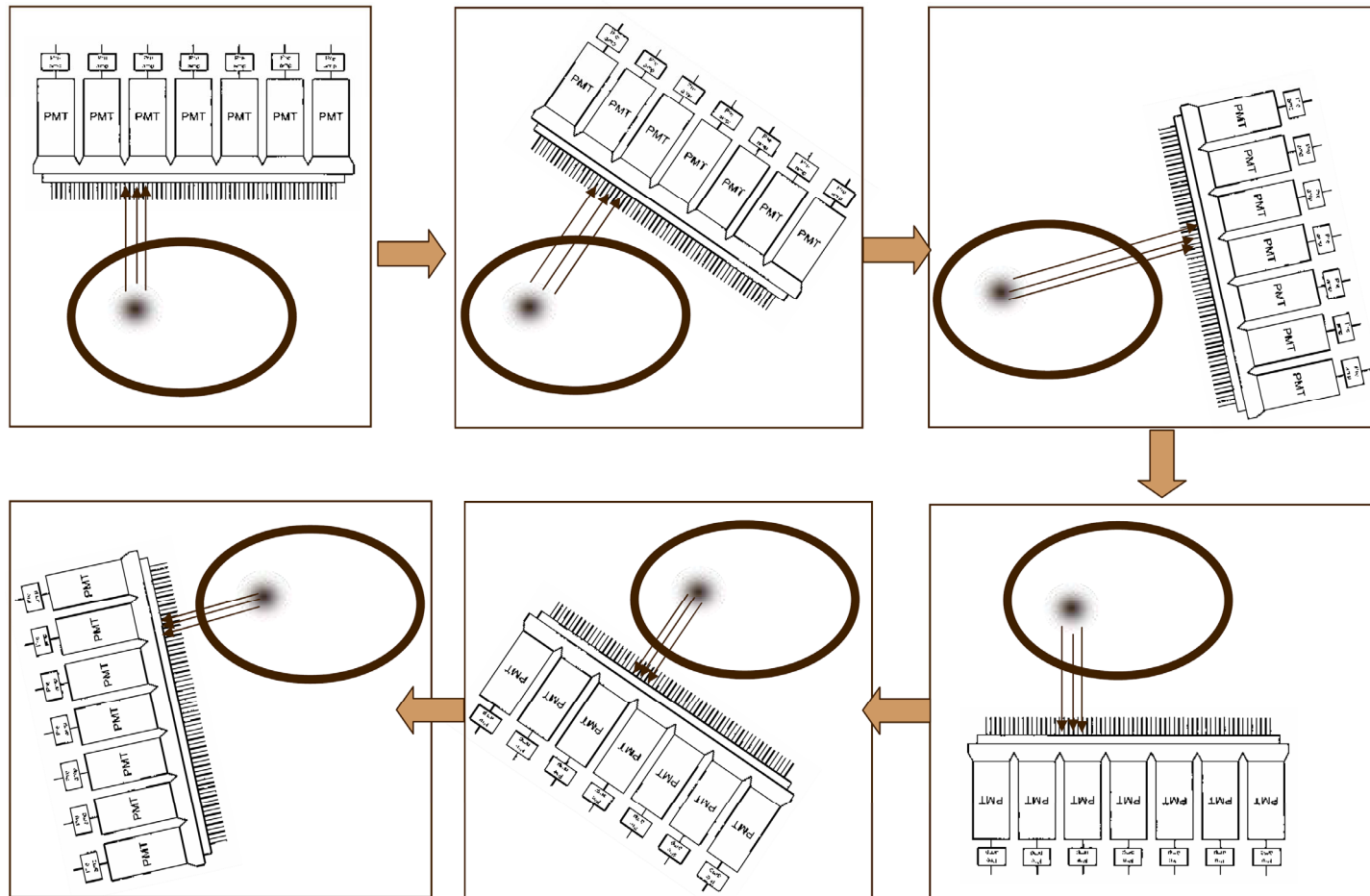
Recent advances: new detector systems, improving the trade-off between spatial resolution & detection efficiency, new radio-labeled pharmaceuticals

# SPECT Basics

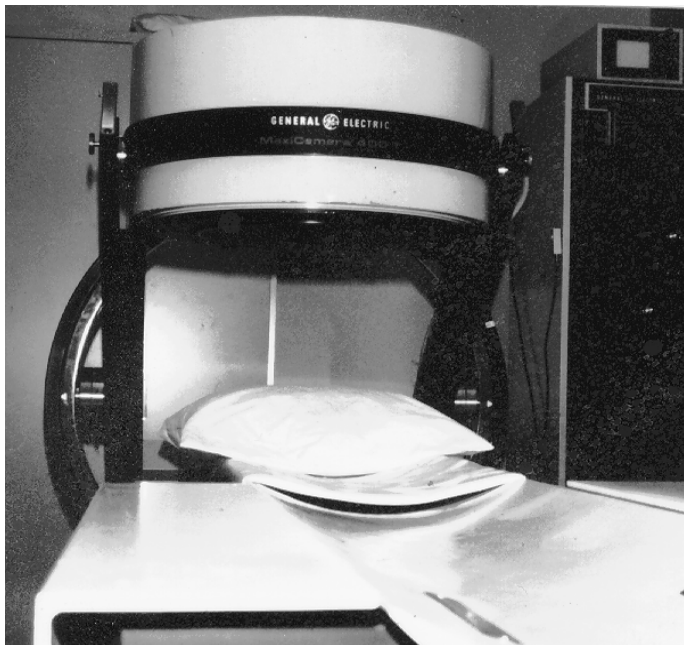


- Sensitive to:  
Tracer (Drug) Concentration
- Contrast:  
Tracer vs. No Tracer
- Advantages:
  - + Visualizes Metabolism
  - + Acceptable Imaging Time
- Disadvantages:
  - Ionizing Radiation
  - Low Resolution

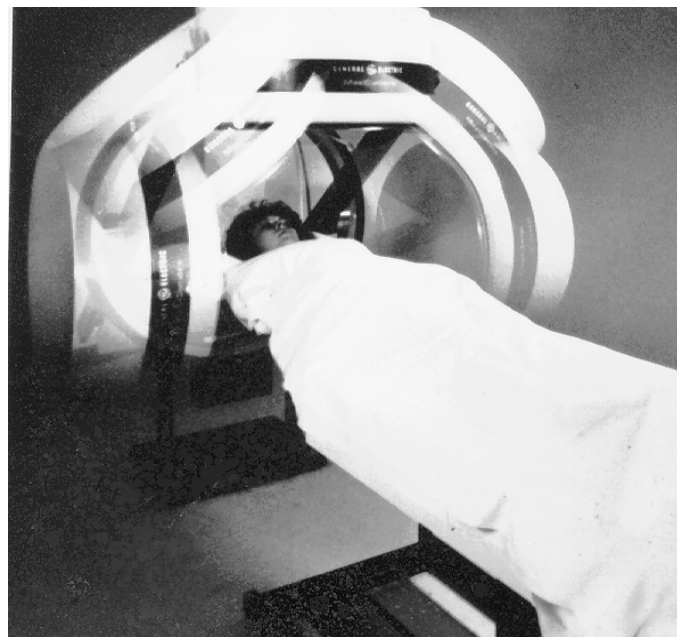
# Basic SPECT – Projection Data



# Early Clinical SPECT



The First Anger Camera



GE 400T Rotating Anger Camera (ca. 1981)

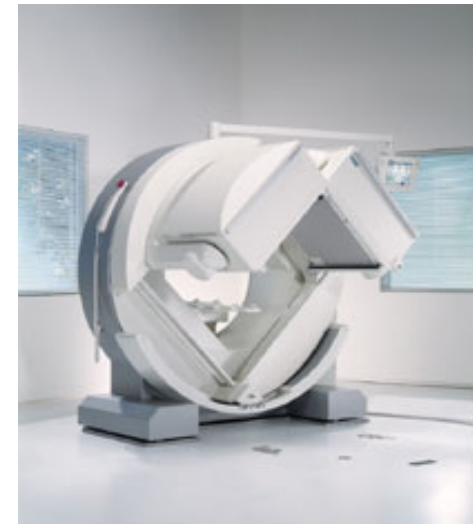
# Modern Clinical Systems



GE Millenium VG

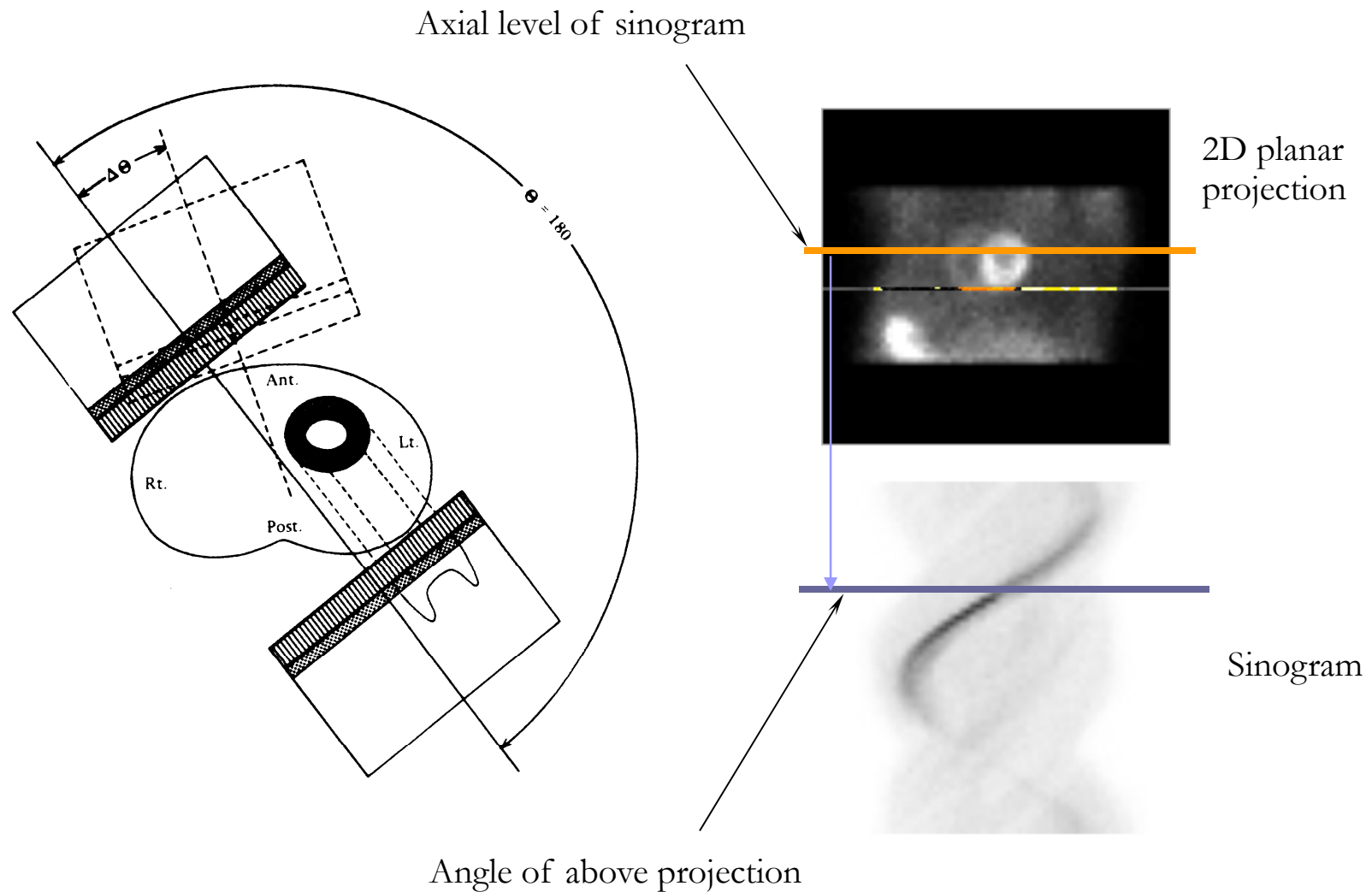


Philips Cardio 60



Siemens e.cam  
Variable Angle

# Basic SPECT – Projection Data



# Simple and Filtered Back-projection

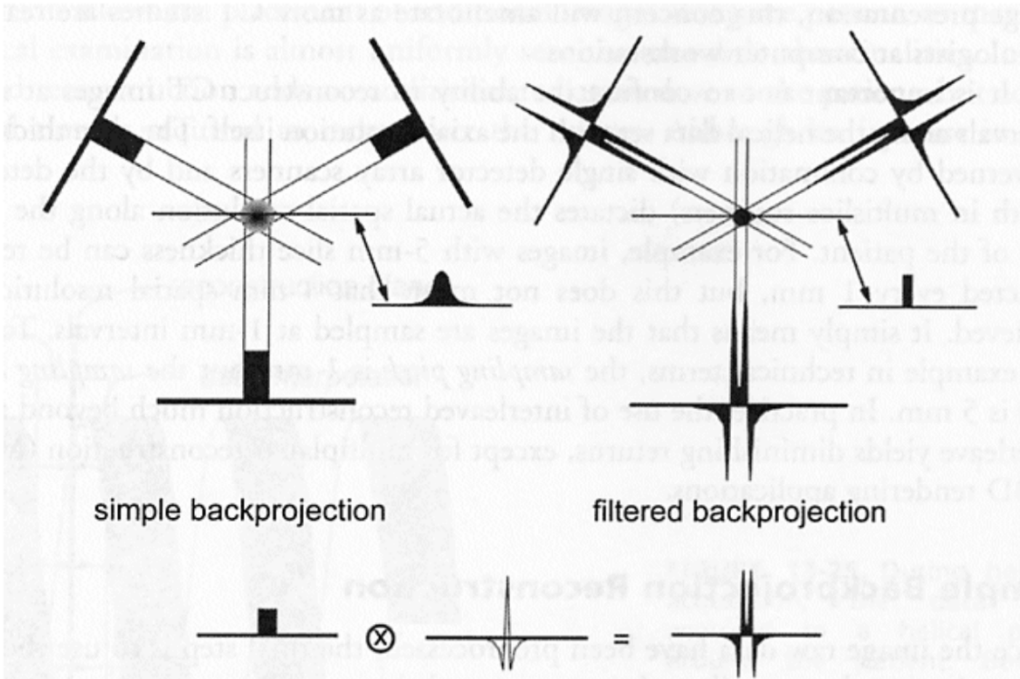
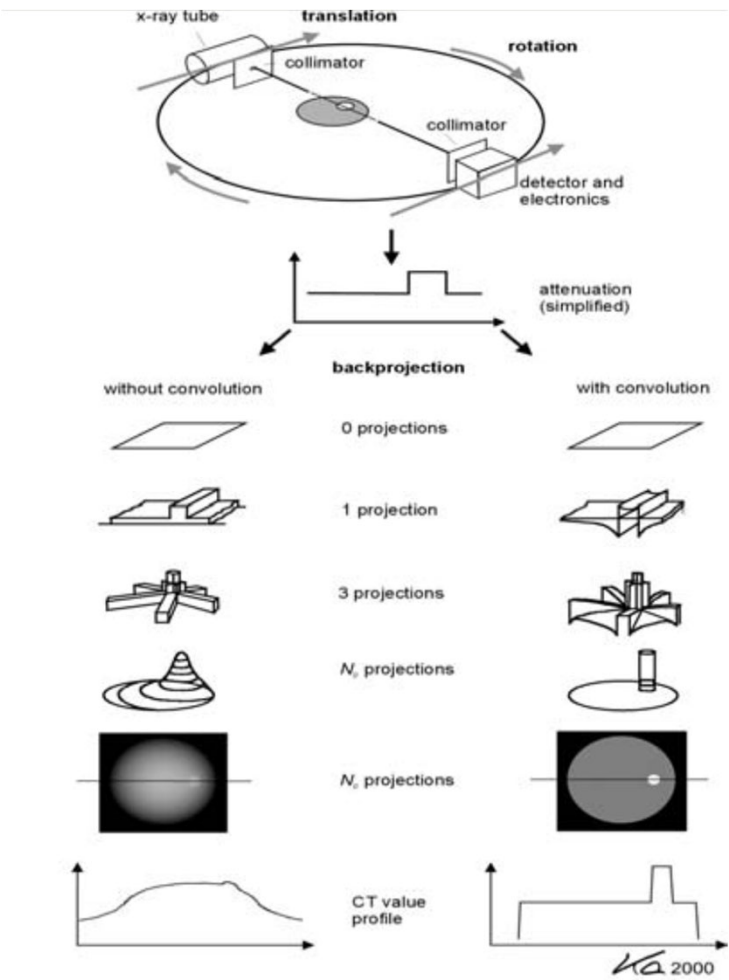


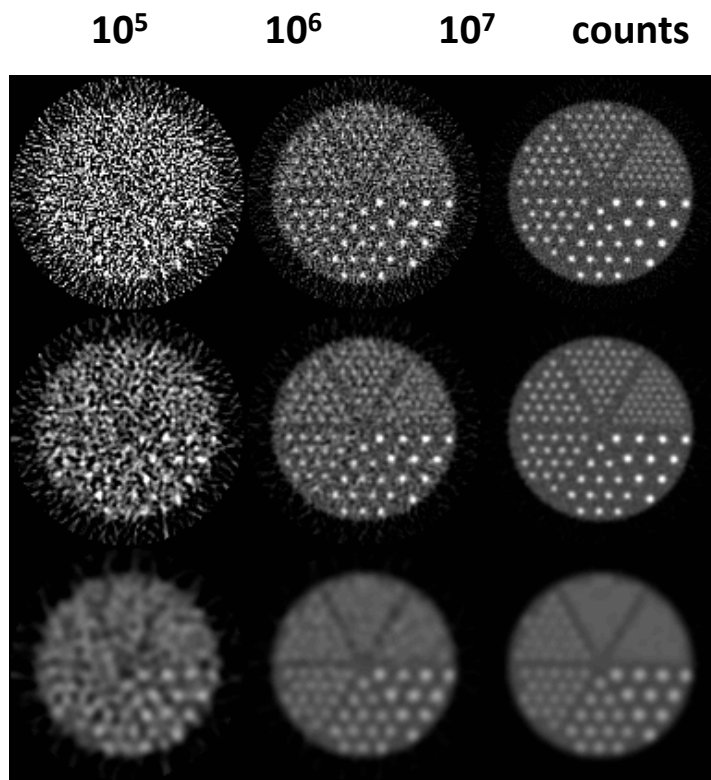
**FIGURE 13-28.** Simple backprojection is shown on the left; only three views are illustrated, but many views are actually used in computed tomography. A profile through the circular object, derived from simple backprojection, shows a characteristic  $1/r$  blurring. With filtered backprojection, the raw projection data are convolved with a convolution kernel and the resulting projection data are used in the backprojection process. When this approach is used, the profile through the circular object demonstrates the crisp edges of the cylinder, which accurately reflects the object being scanned.



Please see Chapter 2 for detailed analysis of image formation and image reconstruction.

# Noise In SPECT Images

- Noise in SPECT images is dominated by the counting statistics of the coincidence events detected.
- Noise can be reduced at the cost of image resolution by using an apodizing window on ramp filter in image reconstruction (FBP algorithm).



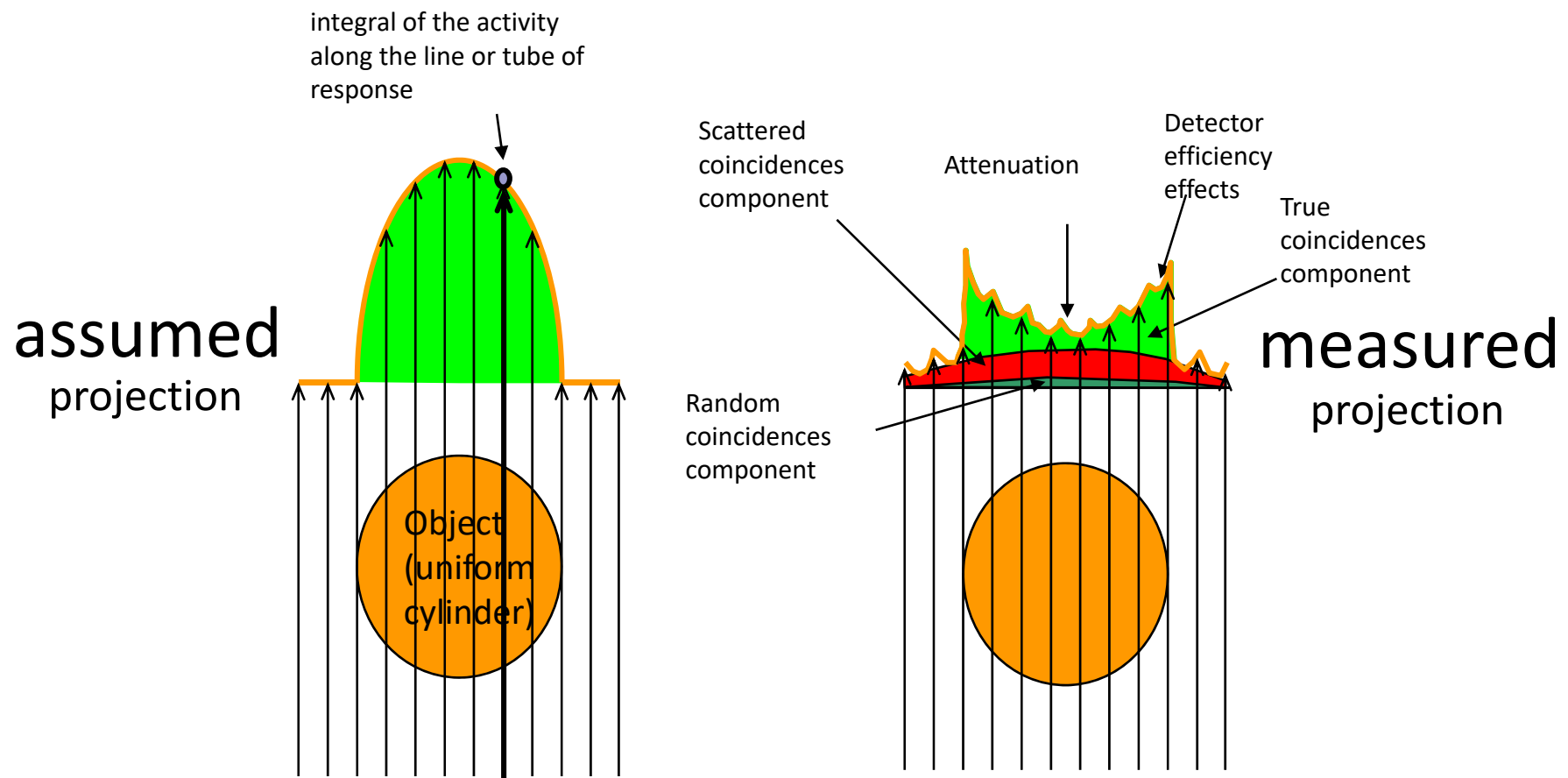
Unapodized ramp filter

Hanning window, 4mm

Hanning window, 8mm

# SPECT image Reconstruction

- Data corrections are necessary
  - the measured projections are not the same as the projections assumed during image reconstruction





# Analytical Methods

- Advantages

- Fast
- Simple
- Predictable, linear behaviour

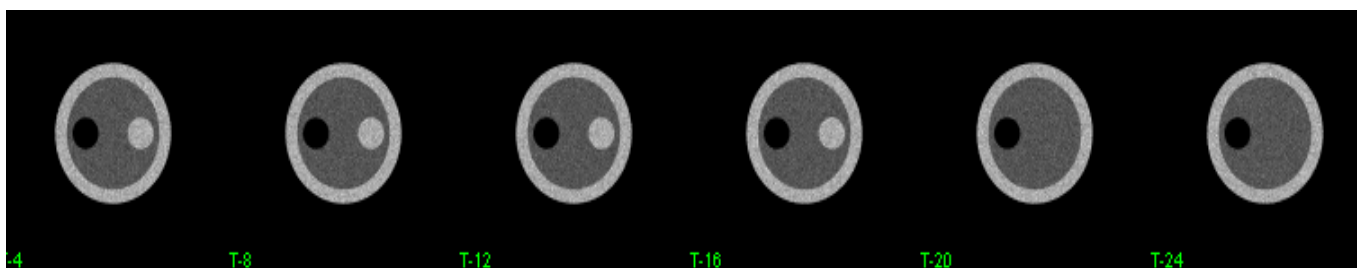
- Disadvantages

- Not very flexible
- Image formation process is not modelled  $\Rightarrow$  image properties are sub-optimal (noise, resolution)

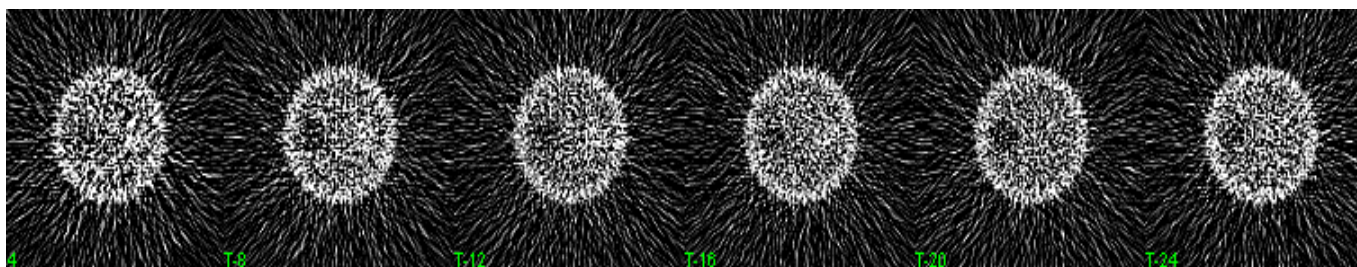
# Problem of Analytical Reconstruction Algorithms

600000 counts (including scatter)

original



3DRP



Hanning

*Image credits:*

*Kris Thielemans*

*MRC CU, London (now IRSL – [www.irsl.org](http://www.irsl.org))*